The Astrophysical Journal, 867:45 (20pp), 2018 November 1 https://doi.org/10.3847/1538-4357/aae08e

Magnetic Buoyancy and Magnetorotational Instabilities in Stellar Tachoclines for Solar- and Antisolar-type Differential Rotation

Peter A. Gilman
High Altitude Observatory, National Center for Atmospheric Research, 3080 Center Green, Boulder, CO 80307-3000, USA; gilman@ucar.edu
Received 2018 July 10; revised 2018 September 5; accepted 2018 September 6; published 2018 October 29

Abstract

We present results from an analytical model for magnetic buoyancy and rotational instabilities in full spherical shell stellar tachoclines that include rotation, differential rotation of either solar or antisolar type, and toroidal field. We find that in all cases, for latitudes where the tachocline vertical rotation gradient is positive, toroidal fields can be stored against magnetic buoyancy up to a limit that is proportional to the square root of the local vertical rotation gradient. For solar magnitude differential rotation, this limit is about 9 kG. For fixed percentage differential rotation, storage capacity varies linearly with the rotation rate. Faster rotators with the same percentage differential rotation can store larger fields, and slower rotators can store smaller fields. At latitudes where the vertical rotation gradient is negative, vigorous magnetorotational instability for even weak ($\ll$1 kG) toroidal fields prevents such storage. We infer from these results that for stars with solar-type latitudinal differential rotation (fast equator, slow poles), any starspots present should be found in low latitudes, similar to the Sun. For antisolar differential rotation, any spots present should be found in mid- and high latitudes, perhaps with a peak of occurrence near 55°. These results hopefully provide some guidance for making and interpreting observations of stellar activity and differential rotation on stars with convection zones and tachoclines.

Key words: instabilities – stars: activity – stars: interiors – stars: magnetic field – stars: rotation

1. Introduction

Magnetic buoyancy and rotational instabilities both have a long history in stellar astrophysics. Generally both are potentially present in stellar interiors, particularly in stars with tachoclines, or sharp rotational shear layers that separate convection zones above from radiatively dominated interiors below (Parker 1955; Gilman 1970; Balbus 1995; Menou et al. 2004; Parfrey & Menou 2007; Davies & Hughes 2011; Mizerski et al. 2013; Kagan & Wheeler 2014). These subjects were recently reviewed in the solar context by Gilman (2018). Gilman (2018) reported on new results for magnetic buoyancy and rotational instability in the solar tachocline. He found that radial rotation gradients in the tachocline prevent magnetic buoyancy in low latitudes, coinciding with the well-known domain of sunspots, until toroidal field peaks reach close to 10 kG. By contrast, in mid- and high latitudes, vigorous magnetorotational instability dominates over magnetic buoyancy instability for toroidal fields as small as 100 G and less. He concluded that these results imply that it would be very hard for the solar dynamo to generate mid- and high-latitude toroidal fields of 1 kG and higher, because they would exit the tachocline and reach the surface too quickly to be stored at tachocline depths for long enough. But magnetorotational instability could be responsible for much smaller scale ephemeral active regions seen there (see, e.g., Yang & Zhang 2014 and earlier references cited therein). In sunspot latitudes, the stabilizing effect of the radial rotation gradient there provides a new, apparently previously unnoticed, mechanism for storing toroidal field produced by the solar dynamo until it amplifies to the point that it can emerge and form sunspots. Taken as a whole, these results might provide a new explanation for why sunspots are found only in low latitudes.

It is clear that these results should be applicable in some form to all the many stars thought to have tachoclines, differential rotation, and dynamos. Much new information about rotation and differential rotation in active stars is becoming available from the *Kepler* and *CoRoT* missions (e.g., Reinhold & Gizon 2015; Valio et al. 2017; Morris et al. 2017). Reinhold & Gizon (2015) show that for magnetically active stars in the *Kepler* sample, the range of both absolute differential rotation and differential rotation relative to the star's minimum rotation is about a factor of 100, for stars that have rotation periods between about 0.5 and 50 days, also a factor of 100. Thus, there are many combinations of rotation and differential rotation that are present in typical stars.

The results we present here are a first effort to apply the missions and solar tachocline model we have developed for magnetic buoyancy and magnetorotational instabilities to the stellar case. The model contains a large number of physical parameters that vary from one star to another, according to its place on the main sequence, its radius, the depth and thickness of the tachocline, and its rotation and differential rotation, among other parameters. Different stars also show different evidence of magnetic activity, and for some there is information about the latitudes of starspots. It is not our purpose here to review the observational evidence for stellar rotation, differential rotation, and magnetic activity. Rather, in this first study we seek to generalize the results of Gilman (2018) to a wide range of "solar"-type stars, for which all physical parameters are the same as for the Sun except differential rotation, which we will vary from zero to 44%, with both signs, so we include solar- and antisolar-type differential rotations both weaker and stronger than Gilman (2018) took for the Sun. We also outline how to use the various dimensionless quantities to estimate results for stars that differ from the Sun in other parameters, such as rotation, radius, mass density, and thickness of the tachocline, as well as toroidal field strength.

2. Summary of Model Development in Gilman (2018)

The eigenvalue equation we will use to study magnetic buoyancy and rotational instabilities in stellar tachoclines with

widely varying differential rotations is identical to that derived for the solar case in Gilman (2018). Full spherical geometry is retained, but the tachocline is assumed to be thin enough that the divergence of radii within the tachocline can be ignored. The centrifugal force from the rotation of the coordinate system (essentially the stellar interior rotation rate, assumed to be constant) is included in the local gravity. Despite being thin, the tachocline model includes a full radial variation in mass density; in other words, the so-called Boussinesq approximation is not invoked. The perturbations are not assumed to be hydrostatic. Perhaps most important, the thermal relaxation time is assumed to be very short compared to viscous and ohmic diffusion times, which is physically well justified for stellar interiors. Stated another way, stellar interior Prandtl numbers are very small compared to unity. Consistent with this property, and as is virtually always done in studies of magnetic buoyancy instabilities, the local perturbations are taken to be isothermal, so there is no perturbation thermodynamic equation to solve. In this case, pressure and density perturbations are directly linked through the equation of state. Consistent with these assumptions, the perturbations are assumed to be very small in scale in latitude, which maximizes the destabilizing effect of magnetic buoyancy. This greatly simplifies the perturbation equations to just four equations for longitudinal and vertical velocities and magnetic fields. These four perturbation equations are then easily reduced to a single quartic algebraic equation that we repeat from Gilman (2018) below.

Definitions of all coordinates, physical quantities, and scaling factors used below are identical to those in Gilman (2018). We summarize them here.

Coordinates: λ, ϕ, z; longitude, latitude, local vertical (dimensionless)

Length scales: R—radius at tachocline depth; D—thickness of tachocline; H—local pressure scale height

Length scale ratios: $\delta = D/R$; $\delta_s = D/H$

Timescale: Ω^{-1}—Ω is rotation rate of coordinate system (stellar interior)

Velocity scales: horizontal velocities by $R\Omega$, vertical velocities by $D\Omega$

Density scale: ρ_{00}, the average density of the tachocline

Density of reference state: ρ_s (function of z only)

Pressure scale: $\Omega^2 R^2$

Magnetic field scales: horizontal fields by $R\Omega/(4\pi\rho_{00})^{1/2}$, vertical fields by $D\Omega/(4\pi\rho_{00})^{1/2}$

Reference state dimensionless variables: ω_0—local rotation relative to Ω; α_0—angular measure of toroidal field; p_0—gas pressure; π_0—total pressure (gas plus magnetic); density function $r_s = 1 + \rho_s/\rho_{00}$. All are functions of ϕ, z except r_s, which is a function of z only.

3. Conditions in Stellar Tachoclines

Before proceeding further, it useful to remind ourselves of the conditions likely to be present in stellar tachoclines, particularly the role of turbulence, and how those conditions relate to our model. Aspects of this issue were discussed in the introduction of Gilman (2018). As widely discussed in the literature, the solar tachocline is thought to contain an upper, or "overshoot," tachocline, slightly subadiabatically stratified, where convective turbulence from the convection zone above penetrates into the shear layer. Below that, there is a "radiative" tachocline, where there is little or no convective turbulence, where the stratification is more subadiabatic. Here the latitudinal differential rotation of the convection zone and overshoot layer above transitions to virtually solid rotation below. Magnetic fields, particularly toroidal, are likely to occupy one or both of these tachocline layers.

Because we are assuming isothermal perturbations for the instabilities of the system, characterized by extremely small latitudinal scale, for which radiation will prevent significant temperature perturbations, the perturbations will feel no negative ordinary buoyancy force, but will still feel magnetic buoyancy, because mass density is directly coupled with gas and magnetic pressure. In this limit, the overshoot and radiative tachoclines will look very similar to a perturbation. In fluid dynamical terms, the system has very small Prandtl numbers (ratio of viscosity or magnetic diffusivity to radiative diffusivity). How might the presence of convective turbulence from overshooting impact this picture? Could the reality be that the effective Prandtl number, due to turbulent transport, is more like unity?

Strictly speaking, only full 3D MHD simulations have the potential to answer such a question, but we can say that the latitudinal scale of convective turbulence is likely to be much larger than we have assumed for the perturbations, which would in effect just render the background state much more complicated, beyond the scope of our study. From mixing length theory (admittedly very crude), we can guess the latitudinal scale of convection to be of order one pressure scale height, or 30–50 Mm. By contrast, the latitudinal scale of unstable flux tubes in a tachocline toroidal field could easily be as narrow as 1 Mm, or even smaller. Estimating the vertical scale of overshooting convection in the overshoot layer requires more sophisticated theory, but it is bounded by the total thickness of this layer, so perhaps 10 Mm, so the same scale argument can be made. In terms of the relative strength of radiative diffusion and turbulent diffusivity of heat, by definition turbulent transport should dominate in the fully convecting region, leading to a turbulent Prandtl number of order unity there. It should also dominate at the top of the overshoot layer, but radiative diffusion will dominate at the bottom of the overshoot layer.

In other words, the overshoot layer contains a transition from turbulent Prandtl numbers of order unity at and near the top to extremely small conventional Prandtl numbers at the bottom. We have not attempted to capture this transition in our instability model, but it could be done. There are other effects to consider in this context. For example, strong toroidal fields are likely to inhibit or even suppress the convective turbulence locally, leading to highly spatially variable turbulent diffusivities, again requiring full 3D MHD simulations to have any hope of understanding. Finally, we have found in the solar case in Gilman (2018) that magnetorotational and even hydrodynamic rotational instability in the isothermal limit is likely to generate turbulence, which will also contribute to modifying the background state away from an idealized nonturbulent layer.

For all these reasons, and to provide continuity with previous studies of magnetic buoyancy and rotational instabilities in stars, in this study we retain the simpler starting point of a nonturbulent background tachocline that contains differential rotation and toroidal fields. This issue of the form of the background state to be perturbed is always present when linearized instability theory is applied to astrophysical or any other fluid systems. The objective of such applications is not to

model the whole system, but rather to gain physical insight into what processes could be important in them, and how they might alter an initial steady background state. Most instabilities lead to turbulence of some form, which must be modeled using techniques that go beyond what mathematical instability theory can provide.

4. Unperturbed States: Family of Solar-like Stars with Widely Varying Differential Rotation

In moving from the solar case studied in Gilman (2018) to the much more general case of instabilities in tachoclines of differentially rotating stars known to have magnetic fields, we need to have a rational way of constraining parameters and physical properties. In this first stellar study, we choose to focus on varying differential rotation. In the solar case the rotation profile we chose had the property of providing an approximate torque balance between the convection zone above and the radiative interior below the tachocline. This choice is made by reference to helioseismic observations, but also by the physical reasoning that, since the exchange of momentum between the solar convection zone and its radiative interior takes place over much longer timescales (essentially the solar "spin-down" time) than momentum exchanges by convective turbulence within the convection zone, there should be such a torque balance. We choose to follow the same reasoning when choosing differential rotation profiles for the current study.

Our unperturbed state contains only differential rotation and toroidal field, together with gas pressure. Other axisymmetric velocities and magnetic fields are set to zero, resulting in a time-independent unperturbed state for latitudinal and vertical force balances. We also find it convenient to introduce angular measures of zonal flow u_0 and toroidal field a_0, such that $u_0 = \omega_0 \cos\phi$, $a_0 = \alpha_0 \cos\phi$. We also define a total pressure $\pi_0 = p_0 + \alpha_0^2 \cos^2\phi$. Then the force balance for the unperturbed state is given by

$$\frac{\partial \pi_0}{\partial \phi} - \alpha_0^2 \sin\phi\cos\phi + r_s(2+\omega_0)\omega_0 \sin\phi\cos\phi = 0, \quad (1)$$

$$\frac{\partial \pi_0}{\partial z} + \delta\alpha_0^2 \cos^2\phi + \delta_s p_0 - \delta r_s(2+\omega_0)\omega_0 \cos^2\phi = 0. \quad (2)$$

Equations (1) and (2) are identical to Equations (24) and (25) of Gilman (2018). By cross-differentiation followed by subtraction of Equation (2) from Equation (1), we can eliminate the total pressure and find the MHD version of the "thermal wind" for this system, which relates the latitudinal gradient of fluid density to latitude and vertical gradients of rotation and toroidal field. This relation is of central importance for studying global instability of such gradients, but we do not have to solve Equations (1) and (2) in the current study.

Equations (1) and (2) contain all the parameters and functions that define the reference state that we will perturb for the instability calculations. We are allowed to specify values for δ and δ_s that are characteristic of the tachocline, as well as the function r_s, which describes the density stratification within the tachocline. These three quantities are not independent of each other, since they all involve the tachocline thickness, so they must be varied together in a consistent way. The quantities ω_0 and α_0, which can be specified independently of δ, δ_s, and r_s, can be functions of both ϕ and z.

The results we present below will be for specified profiles of differential rotation and toroidal field. In the absence of more detailed guidance from observations, we will assume that differential rotation is linear in z, as we did for the solar case in Gilman (2018), in the form

$$\omega_0 = (s_0 + s_2 \sin^2\phi + s_4 \sin^4\phi)z, \quad (3)$$

in which we will take s_0, s_2, s_4 in a fixed amplitude ratio. The differential rotation ranges from zero at the bottom of the tachocline at $z = 0$ to its maximum at the top at $z = 1$, for both solar- and antisolar-type differential rotations. For solar-type differential rotation, $s_0 > 0$, s_2, $s_4 < 0$; antisolar profiles have the opposite signs for each of these parameters. We specify $s_2 = s_4$ in all cases and keep the ratios of both to s_0 fixed, so that for all cases the vertical rotation gradient changes sign at the same latitude, approximately 32°.3. This choice satisfies our constraint chosen above that there be a balance of torques between the convection zone above and the radiative interior. Obviously other profiles can also be studied. In particular, as a function of stellar rotation, there may be a transition between solar and antisolar differential rotation that takes the form of maximum angular velocity at midlatitudes rather than at either the equator or the poles. But we can infer what happens in this case from the solar and antisolar cases.

We should also keep in mind regarding these instabilities in stars that we are specifying the differential rotation in and across the stellar tachocline, but not in the convection zone or stellar photosphere above. Unlike the Sun, any observations of stellar differential rotation are for the stellar surface. In the Sun, we know from helioseismic measurements that at least 80% of the surface differential rotation is present at the top of the tachocline. It is plausible to assume that this will also be true for other solar-type stars with similar rotation and age. But younger and older stars with very different rotations could be different. Some limited guidance can be sought from stellar differential rotation models for convection zones. Intuitively, it does seem unlikely that latitudinal differential rotation at the depth of the tachocline could actually be larger than at the stellar surface, because it is easier for rotationally induced Reynolds stresses in the convection zone to produce differential rotation where the mass density and therefore rotational inertia are so much smaller.

We will also do calculations for constant rotation ($f = 1$) where we set s_0, s_2, $s_4 = 0$, to see the effect of constant rotation at different latitudes on magnetic buoyancy instability.

For the toroidal field we will consider a quadratic profile of the form

$$\alpha_0 = \alpha_{00} z(1 - z), \quad (4)$$

which peaks at mid-depth in the tachocline and is zero at its bottom and top. Obviously other profiles are possible, including linear combinations of that in Equation (51) and a constant field, but we feel we capture the essential behavior with these two cases. We have also done a few calculations with constant toroidal field to assess the effect of a uniform field on instability of the differential rotation.

5. Eigenvalue Equation to Be Solved

As given in Gilman (2018), the perturbation eigenvalue equation for unstable disturbances is found by assuming that all

independent variables are proportional to $e^{i(m\lambda+n\phi-\tau t)}$, in which m is the longitudinal wavenumber, n is the latitudinal wavenumber, and τ is the complex eigenvalue (τ_i is the growth rate, and τ_r/m is the phase speed). After algebraic reduction described in Gilman (2018), the complex eigenvalue can be found from a single quartic algebraic equation, Equation (46) of Gilman (2018), which is

$$(m\omega_0 - \tau)^4 + a_q(m\omega_0 - \tau)^2 + b_q(m\omega_0 - \tau) + c_q = 0, \quad (5)$$

in which

$$a_q = -\frac{2m^2\alpha_0^2}{r_s} - \frac{\alpha_0\cos^2\phi}{\delta r_s}\left(\frac{\delta_s}{\delta} - 2\right) \times \left(\frac{\partial\alpha_0}{\partial z} - \left(\frac{1}{r_s}\frac{\partial r_s}{\partial z} + \delta\right)\alpha_0\right) - \frac{2\cos^2\phi}{\delta}(f + \omega_0)\left(\delta(2f + \omega_0) + \frac{\partial\omega_0}{\partial z}\right), \quad (6)$$

$$b_q = -\frac{2m\cos^2\phi\alpha_0^2(f + \omega_0)}{r_s}\left(\frac{\delta_s}{\delta} - 2f(1 + \delta) - \frac{1}{r_s}\frac{\partial r_s}{\partial z}\right), \quad (7)$$

$$c_q = \frac{m^4\alpha_0^4}{r_s^2} + \frac{m^2\alpha_0^2\cos^2\phi}{\delta r_s}\left(\left(\frac{\delta_s}{\delta} - 2\right)\frac{\alpha_0}{r_s}\left(\frac{\partial\alpha_0}{\partial z} + \delta\alpha_0\right) + 2f(1 + \omega_0)\left(\frac{\partial\omega_0}{\partial z} - \delta\omega_0\right)\right). \quad (8)$$

In the definitions of a_q, b_q, c_q we have added a "flag," denoted by f, which marks the places in the equations of the dimensionless rotation of the system. When rotation is included, $f = 1$; when it is absent, $f = 0$. This allows us to use the same formulae for the case with no rotation, to calculate magnetic buoyancy instability from the same formulae in the nonrotating case (obviously the differential rotation can be switched off by setting $\omega_0 = 0$ everywhere). Two limiting cases are important: when there is no rotation and no differential rotation, and when there is no toroidal field. With no rotation, Equation (5) becomes quadratic in τ^2; when there is no toroidal field, one $(m\omega_0 - \tau)^2$ factors out, and the rest yields a quadratic equation for $(m\omega_0 - \tau)$. This is because in both cases $b_q = 0$.

It is well known that analytical solutions exist for quartic equations. As in Gilman (2018), we use the forms described in the Handbook of Mathematical Tables and Formulas by Burington (1953), an admittedly ancient, but reliable, source. These solutions work even in the special cases of zero rotation or zero toroidal field, yielding answers very close to those from the corresponding quadratic forms in these cases, a useful check on the general forms and our FORTRAN codes, each of which was written independently for the general and special cases. As a further check, for the general case we also found sample solutions from the general Equation (5) by minimizing its left-hand side by scanning through eigenvalue space, using as guidance for the scan the analytical solutions found. Agreement was very good in all cases tried.

In brief, as documented in Burington (1953), quartics are solved by finding the roots of the "resolvent cubic," whose coefficients are related algebraically to the quartic coefficients. The roots of the quartic are sums and differences of square roots of the resolvent cubic's roots. From the details of the analytical solutions in Burington's tables, we can see that unstable modes are guaranteed only when the quantity $H = b_r^2/4 + a_r^3/27$ is positive. The quantities a_r, b_r are related to a_q, b_q, c_q in Equations (5)–(8) by $a_r = -a_q^2/48 - c_q/4$ and $b_r = (-a_q^2/108 + a_q c_q/3 - b_q^2/8)/8$. All unstable modes we find have $H > 0$. In principle, we can find the boundaries of unstable domains in our parameter space by solving the equation $H = 0$. Given the complexity of the algebra involved, this is impractical; instead, we find the stability boundaries, where they exist, by approaching them from an adjacent unstable domain.

It is important to recognize that Equations (5)–(8) are valid locally for all latitudes and vertical elevations, and for all profiles of differential rotation and toroidal field, and for all stratifications, as represented by r_s. This means that, even if all parameters in Equation (5) are independent of z, the eigenvalue itself is still a function of z. As a result, the form of the eigenfunction is not known, though we can get guidance on what its profile with z is likely to be from the profile of growth rate τ_i with z. This issue is discussed at length in Mizerski et al. (2013). They show that in the Cartesian nonrotating case, at least there is a close correspondence between the local instability results such as we have found here and the full two-point boundary value eigenvalue problem. It is likely, though not yet proven, that the same is true for the rotating, spherical case we analyze here; it remains a research problem for applied mathematicians. In Section 5, Gilman (2018) discussed this issue further. It has been a question to consider throughout the history of magnetic buoyancy instability studies. In practical terms, in an initial value calculation for instability, we expect that a smooth perturbation profile will develop whose growth rate is close to that of the maximum growth rate of the the eigenfunction from the solution of the eigenvalue problem.

Equations (5)–(8) also apply for a wide range of tachocline thicknesses as measured by δ, δ_s. Within the approximations we have made, and in the limit $n \to \infty$, δ, δ_s can even vary with latitude. In addition, they also apply for essentially any profiles of toroidal field and differential rotation with both latitude and depth, so the system can be applied to the tachocline of virtually any hypothetical or real star.

6. Hydrodynamic Rotational Instability and Restoring Forces for Solar- and Antisolar-type Differential Rotation

In our system, even if there is no toroidal field, there can still be instability because there is differential rotation. We can find the eigenvalues for neutral and unstable modes either from Equations (42) and (43) of Gilman (2018) directly or from Equations (5)–(8) in the limit of $\alpha_{00} \to 0$. Either way, the reference state density parameter r_s is absent, so these results are independent of density effects, and therefore the same in Boussinesq and non-Boussinesq regimes. The reduced equation with nontrivial solutions for instability is a simple quadratic, given by

$$(m\omega_0 - \tau)^2 = 2\cos^2\phi(1 + \omega_0)\left(2 + \omega_0 + \frac{1}{\delta}\frac{\partial\omega_0}{\partial z}\right), \quad (9)$$

whose roots are

$$\tau = m\omega_0 \pm \cos\phi\left(2(1 + \omega_0)\left(2 + \omega_0 + \frac{1}{\delta}\frac{\partial\omega_0}{\partial z}\right)\right)^{\frac{1}{2}}. \quad (10)$$

Equations (9) and (10) are identical to Equations (52) and (53) of Gilman (2018) where only the solar case was considered. Clearly we get a complex eigenvalue, signifying instability, only when the argument of the square root in Equation (10) is negative. We also see that a component of the real part of τ/m, which is the phase velocity of the mode, whether neutral or unstable, is just the passive advection of the perturbation in longitude at the speed of the local rotation rate ω_0 (the term $m\omega_0$). All unstable modes have this phase speed. When the argument of the square root is positive, then we have all neutral wave modes, which come in pairs, with an additional restoring force that creates a total phase speed that is either greater than or less than the local rotation speed by the same amount. These represent a form of inertial oscillation, determined locally by the combination of Coriolis forces in the rotating frame (the terms inside the square root that do not contain ω_0), Coriolis and centrifugal forces from the local rotation ω_0 relative to the rotating frame, and inertial forces from the local vertical rotation gradient. This oscillation is maximum at the equator and zero at the poles, from the factor $\cos\phi$ in front of the square root. It is clear from Equation (10) that for all but the smallest vertical rotation gradients the last term in the brackets on the right-hand side dominates in determining the size of this restoring force, so this force is proportional to the square root of the vertical rotation gradient.

Coriolis forces from the rotating frame are the same for solar- and antisolar-type differential rotation, but all the other inertial forces have differing amplitudes and signs at low and high latitudes according to whether the differential rotation is of solar or antisolar type. Stated another way, solar type ω_0 is positive in low latitudes and negative in mid- and high latitudes, while antisolar type ω_0 is the opposite. Therefore, we should expect the solutions for τ from Equation (10) to look rather different in the two cases. We illustrate this difference in Figure 1, which displays the restoring force for neutral oscillations at the latitudes where they occur, together with the growth rate, or destabilizing force, for modes at latitudes where instability occurs. We chose a total differential rotation of ± 0.28, to compare the solar-type differential rotation used in Gilman (2018) with an antisolar profile of the same size. For comparison, we also include the restoring force for the case of zero differential rotation.

Figure 1 illustrates clearly how different the three cases are, in terms of restoring forces and instabilities. Only the solar-type differential rotation profile shows any instability. Since with no differential rotation there is no energy source available to drive instability, it is not surprising that there is a restoring force at all latitudes in that case. As stated earlier, this force is maximum at the equator, zero at the poles, and proportional to $\cos\phi$ at all latitudes. By contrast, with antisolar differential rotation, the restoring force is weaker than without differential rotation at low latitudes, but stronger than without it at mid- and high latitudes. The opposite is true for solar-type differential rotation. As discussed in the legend for Figure 1 in more detail, we can plot growth rate and restoring force as different segments of the same curve, since they represent solutions to the same equation at different latitudes.

The size of the restoring force we see in Figure 1 tells us how large a magnetic buoyancy we must have for it to overcome the restraint of the inertial forces. For solar-type differential

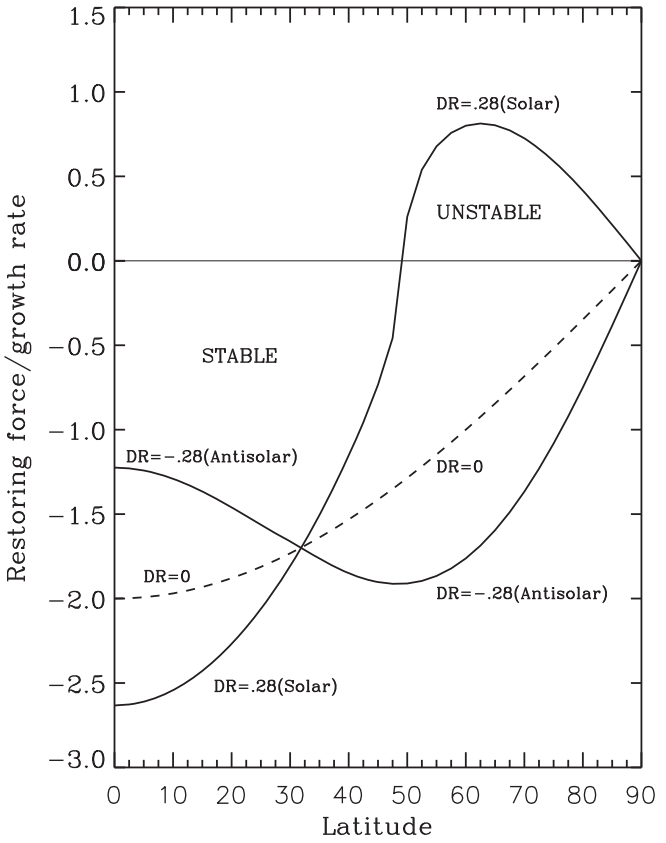

Figure 1. Dimensionless growth rates (positive values) and restoring force amplitudes (negative values) of linear modes in the spherical shell with rotation and differential rotation but with no toroidal fields. We can plot the seemingly different physical quantities "growth rates" and "restoring force amplitudes" as different segments of the same curve, because they come from two different solutions (Equation (10)) to the same equation (Equation (9)), but with opposite signs, whose solutions do not overlap in latitude. Although not standard instability terminology, we could have called the growth rate "destabilizing force," to make it parallel with "restoring force."

rotation, the buoyancy force must be largest in low latitudes, while any destabilizing magnetic buoyancy only adds to instability in high latitudes. By contrast, for antisolar differential rotation, magnetic buoyancy must be significantly larger in mid- to high latitudes, centered around 50°, than near the equator. It is clear from Equation (10) that for all but the smallest vertical rotation gradients, the last term in the brackets on the right-hand side dominates in determining the size of this restoring force, so this force is proportional to the square root of the vertical rotation gradient. Thus, the magnitude of inertial force magnetic buoyancy must overcome increases as the square root of the vertical rotation gradient. So the peak field that can be stored should increase in the same way. Our results below verify that this is indeed the case for both solar- and antisolar-type differential rotation.

How typical are the cases with differential rotation shown in Figure 1? For solar-type differential rotation, Figure 2 shows the same plot for a whole family of solar-type differential rotations between 0 and 0.44. We see that both the restoring force and the growth rates monotonically increase with differential rotation. But there is a threshold of differential rotation of this type, at about 0.10, below which there is no instability at any latitude. Thus, for lower differential rotations, even at high latitudes the stabilizing effect of the Coriolis force

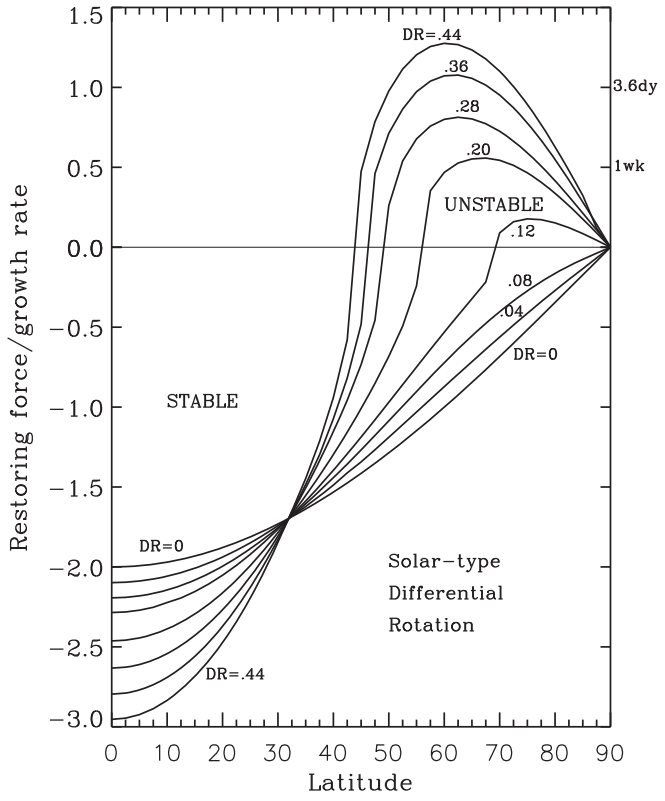

Figure 2. Dimensionless growth rates (positive values) and restoring force amplitudes (negative values) of linear modes in the spherical shell with rotation and solar-type differential rotation but with no toroidal fields. The right-hand scale for positive values gives dimensional *e*-folding growth times for unstable modes. See Figure 1 legend for discussion of growth rates and restoring force being part of the same curve.

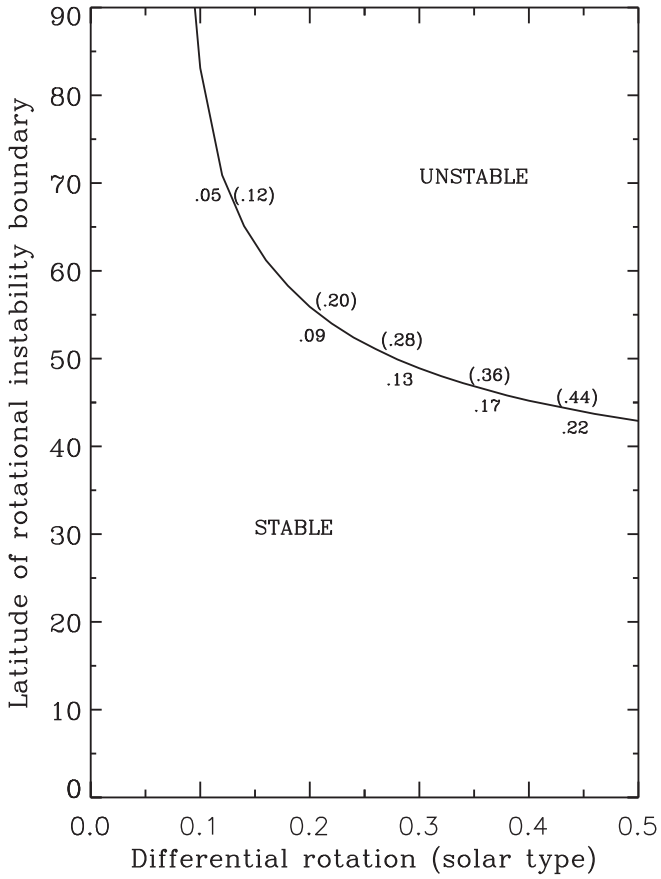

Figure 3. Latitude of boundary poleward of which there is rotational instability as a function of solar-type differential rotation amplitude. Numbers in parentheses are a sample of differential rotation amplitudes for which high-latitude tachocline thickness must expand to avoid instability. Thickness required at the pole, in units of fraction of the tachocline radius, are shown without parentheses below the boundary curve.

of the reference frame prevents the radial rotation gradient from becoming unstable. The latitude poleward of which there is instability migrates toward the pole, as depicted in Figure 3. In this figure, numbers in parentheses are the total differential rotations; numbers below the curve are the thickness of the tachocline at the pole required to eliminate the instability all the way to the pole, by reducing the radial rotation gradient for the same rotation difference across the tachocline. In Gilman (2018) we argued that for the solar differential rotation we assumed, guided by helioseismic measurements, the tachocline thickness at high latitudes, where it is not easily observed using helioseismology, should be much thicker than in low latitudes.

Figure 4 shows the corresponding restoring force for antisolar differential rotations over the same range of values as Figure 2 shown for solar types. Here we see that at mid- and high latitudes, increasing differential rotation increases the restoring force that magnetic buoyancy would have to overcome, while in low latitudes the opposite is true. But unlike for solar-type differential rotation, one has to go to much higher differential rotations to get any instability at all, and then it occurs only very near the equator. We are unaware of any real star reported to have an antisolar differential rotation of this magnitude. In the antisolar case there is no theoretical indication that the tachocline should be any thicker in low latitudes owing to turbulence from rotational instability there.

The physical interpretation of the instability and restoring forces we have found is as follows. For both solar and antisolar differential rotations, moving fluid elements are always conserving their total angular momentum, because there are no longitudinal pressure forces even when $m > 0$. This is a direct consequence of taking the limit of $n \to \infty$, standard in magnetic buoyancy instability studies, which is itself consistent with the assumption of infinitely fast thermal relaxation. Perturbations are always working against Coriolis forces, which are proportional to $\cos\phi$, and so are largest at the equator, zero at the poles. Whether a particular latitude has rotational instability is determined by the local radial gradient of rotation. If it is sufficiently negative, a radially moving fluid element arrives at a new location with higher angular velocity than its local surroundings, and so it keeps going in the same direction owing to local centrifugal forces. This is easier to achieve for solar-type differential rotation, which has a negative radial rotation gradient in high latitudes and only a weak local Coriolis force to work against. By contrast, for antisolar differential rotation the negative radial rotation gradient is in low latitudes where the opposing Coriolis force is much stronger, requiring an even stronger negative rotation gradient to generate instability. On the boundary for rotational instability of solar-type differential rotation shown in Figure 3, there is an exact balance between local centrifugal and Coriolis forces, so the disturbances are marginally stable.

7. Magnetic Buoyancy Instability without and with Rotation

Pure magnetic buoyancy instability without and with uniform rotation was studied in spherical geometry by Gilman (2018).

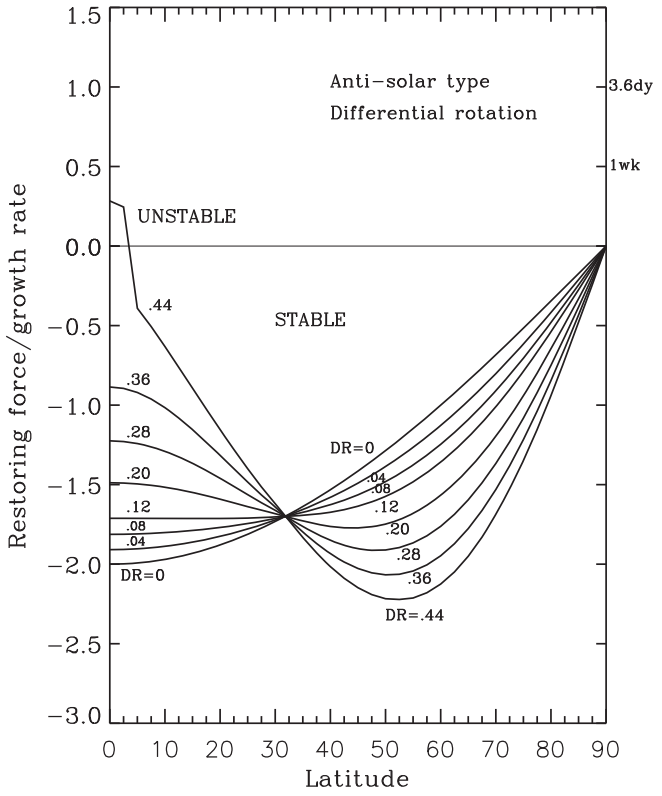

Figure 4. Same as Figure 2, but for antisolar-type differential rotation profiles.

Since we need these results as a comparison point for discussing results for both solar and antisolar differential rotations, we summarize them here. Certain aspects will also be present in some later figures.

With no rotation, magnetic buoyancy instability is depicted in Figure 3 of Gilman (2018), which gives growth rates for all latitudes and longitudinal wavenumber m between 0 and 15. These are calculated for a peak toroidal field of 10 kG, using the same toroidal field profile as specified in Equation (4) here, but apply to all field strengths by simple linear scaling. This reflects the result that without rotation toroidal fields are unstable for all peak field strengths and all latitudes. The instability is confined to the upper half of the toroidal field distribution ($0.5 < z < 1.0$), where the vertical gradient of toroidal field is negative. The $m = 0$ mode is always the most unstable, but only slightly so in low and midlatitudes. The higher the latitude of the toroidal field peak, the faster the growth rate falls off with m. For each latitude there is a high-m cutoff to the instability, $m \gg 15$ for low and midlatitudes, and $m < 15$ for latitudes poleward of about 84°. What causes this is that as m increases at any latitude, the magnetic stress due to the bending of perturbation field lines, which opposes the perturbation magnetic buoyancy, gets larger, while the magnetic buoyancy does not. The higher the latitude, the shorter is the circumference, so for the same m the larger is the magnetic stress owing to larger local curvature of field lines. Without rotation, the longitudinal phase velocities of all unstable modes are zero, regardless of latitude or toroidal field strength. Therefore, modes unstable due to magnetic buoyancy are in no sense Alfvén waves propagating in longitude.

When solid rotation is added to the system (see Figure 4 of Gilman 2018), all latitudes are still unstable for all peak toroidal fields, but Coriolis forces reduce the growth rates, by an amount that is maximum at the equator and declines to zero at the poles. The Coriolis force is also most stabilizing for low wavenumbers because these modes show the strongest tendency to conserve angular momentum, while at the same time experiencing the weakest magnetic stress. As a result, unlike the nonrotating case, the most unstable m is not zero, but itself a function of latitude, declining for a given peak toroidal field from a maximum at the equator to zero near the poles. At the poles, even though the system is rotating, the Coriolis force in radial and longitudinal directions is zero. As the toroidal field peak is raised while holding the latitude fixed, the m for maximum growth rate itself declines, because as the toroidal field rises, magnetic buoyancy grows relative to the stabilizing Coriolis force, until by 20 kG the most unstable mode is for $m = 0$ at all latitudes, as in the nonrotating case. Unlike in the case without rotation, unstable modes with solid rotation do have a longitudinal phase speed, one that is positive, that increases to a limiting value (about 1.5% above the rotation rate) as the toroidal field is increased. As discussed in Gilman (2018), these appear to be a form of slow magnetorotational wave.

8. Magnetic Buoyancy and Magnetorotational Instabilities for Solar-type Differential Rotation

A principal result of Gilman (2018) was to show that for the solar differential rotation the tachocline became unstable to magnetic buoyancy only when the toroidal field was raised above a threshold value, about 9 kG at the equator, declining to zero at the latitude where the radial rotation gradient changed sign, about 32°.3 for the profile chosen. Gilman (2018) reasoned that this result supported an additional mechanism for holding dynamo-generated toroidal fields in the tachocline long enough to amplify to the point that when they erupt and rise to the photosphere, they are strong enough to create sunspots. This could provide a new explanation for why sunspots are seen only at low latitudes. Here we present the same calculation for a wide range of solar-type differential rotations. Figure 5 shows the result. We see that we get a similar effect in the same latitude range for all differential rotations chosen. In fact, the threshold for instability does not drop to zero until the differential rotation itself is taken to be zero, which would take us back to Figure 4 of Gilman (2018). By eye, we can see in Figure 5 that the threshold toroidal field increases roughly as the square root of the differential rotation. We return to this point in Section 10, where we discuss similarities and differences between solar and antisolar cases. Thus, we have shown that the low-latitude inhibition of magnetic buoyancy instability by the radial rotation gradient is a universal feature, present to varying degrees where the radial rotation gradient is positive. Figure 5 also indicates that poleward of the latitude where the radial rotation gradient changes sign, we get magnetorotational instability, which we return to later in this section.

What wavenumbers experience magnetic buoyancy instability, and how fast do they grow, as a function of differential rotation? In the four frames of Figure 6 we sample growth rates as functions of m for four choices of differential rotation, 0.28, 0.08, 0.02, and 0.00 at latitude 15°, roughly in the middle of the latitude domain where differential rotation is stabilizing. For purposes of comparison, we have deliberately used the same vertical scale range in all four figures, even though in two cases very slowly growing modes fall off the bottom of the vertical

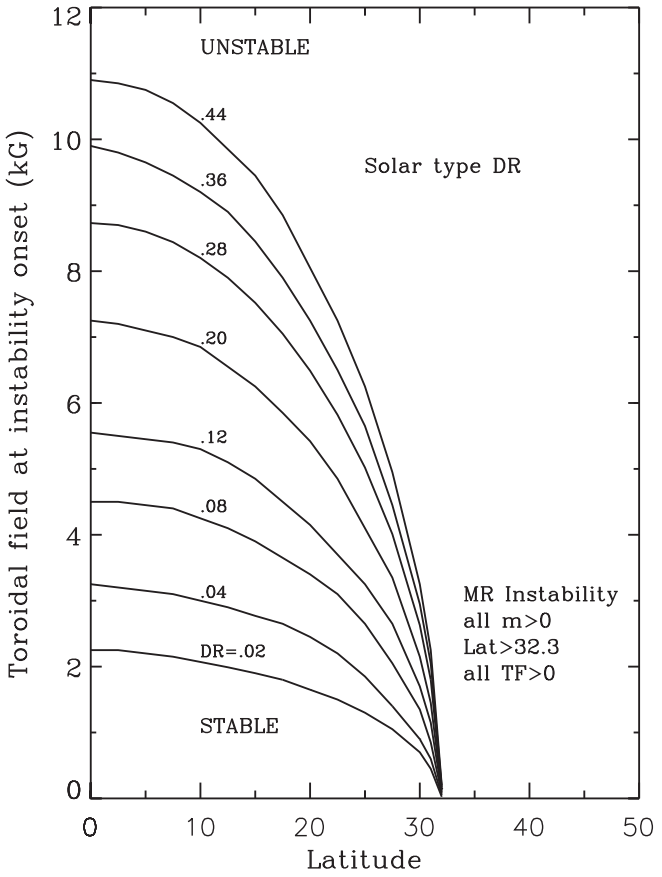

Figure 5. Threshold toroidal field for magnetic buoyancy instability as a function of latitude for a range of solar-type tachocline differential rotations.

scale, which is set at an *e*-folding growth time of 10 yr, so long as to be ineffective in changing the toroidal field in the Sun on a timescale very short compared to a sunspot cycle, which is essential for influencing the dynamo-generated toroidal field.

Each frame of Figure 6 shows how the range of unstable m and the m of peak growth rate vary as the toroidal field is raised. For all cases with nonzero differential rotation, $m = 1$ is the first mode to become unstable; for each case, above the instability threshold the m with the largest growth rate rises to a maximum and then descends to zero for toroidal fields of 20 kG, for which the magnetic buoyancy effects totally dominate over those of rotation and differential rotation. How high m is for the most unstable mode for intermediate toroidal fields is itself a function of differential rotation amplitude. Higher differential rotations favor lower most unstable m's. For all nonzero differential rotations, we also find that as the toroidal field is raised above the threshold for instability, the domain in z that is unstable expands to higher and lower z from about $z = 0.8$, reaching limits of $z = 0.5$ below and $z = 1$ above, consistent with the requirement that the vertical gradient of toroidal field be negative for instability. (See Figure 7 in Gilman 2018 for details of the profiles of growth rate with z for the solar differential rotation of 0.28.) The location near $z = 0.8$ is favored at threshold because that is the location of the maximum negative value in the vertical gradient of the toroidal magnetic field energy. With zero differential rotation the most unstable m for all toroidal fields except the largest is much higher than $m = 15$, though the growth rate curves are nearly flat with m. In each case, the $m = 0$ mode is not unstable for toroidal fields less than about 12 kG, consistent with previous results in Gilman (2018) and in Gradski & Mizerski (2018). In all cases, $m > 0$ modes are the most unstable for lower field strengths, but $m = 0$ is most unstable for high toroidal fields.

We already know from results in Gilman (2018) that with zero differential rotation there is magnetic buoyancy instability present at all latitudes for all peak toroidal fields. Furthermore, the most unstable m is the same for all weak toroidal fields; at 15° it is $m = 11$. So what happens as differential rotation is decreased toward zero, but still slightly above it? For a given very weak differential rotation, a declining peak toroidal field always reaches a level where magnetic buoyancy is stabilized; the first m above that field that is unstable is always $m = 1$. One can argue that this limit is singular in m, in the sense that when differential rotation is zeroed out, the system is still unstable, but the most unstable mode number jumps to the value determined by setting differential rotation to zero in advance. This issue of singular limits comes up again when we consider the case of magnetorotational instability that dominates at high latitudes with solar-type differential rotation. It is also present for antisolar-type differential rotations.

Since stellar dynamos are usually supplying the toroidal field and magnetic buoyancy instability will limit its amplitude, given these results, it is hard to see how, for all but the highest latitudes, the $m = 0$ mode ever becomes unstable, since magnetic buoyancy instability should bound the amplification of toroidal fields by dynamo action. From Figure 6, it is clear that for all nonzero differential rotations, magnetic buoyancy instability should generate a rather broad spectrum of modes with different m. Nonlinear simulations would be required to determine the relative amplitudes of modes in this spectrum. Such simulations are well beyond the scope of this study. It is remarkable that, for such a wide range of differential rotations, the overall patterns of growth rate with longitudinal wavenumber are so similar. The principal difference is just the differing thresholds for onset of instability. In each case, *e*-folding growth times become significantly less than a month for peak toroidal fields of 4, 5.5, and 8.5 kG for differential rotations of 0.02, 0.08, and 0.28, respectively. These times are consistent with times estimated from numerical simulations for a loop of toroidal flux entering a stellar convection zone from below to reach the visible surface. Presumably the toroidal field achievable by dynamo action will be limited by the capacity of the dynamo to generate new toroidal field at least as fast as it exits the tachocline and rises to the surface in loops. Given that the sunspot cycle period is about 11 yr, and cycle periods of most stars where it has been observed are also several years, *e*-folding growth times of just a few days, which we see in Figure 6 for toroidal fields of magnitude 12 kG and higher, should rather quickly overpower the dynamo's ability to regenerate toroidal field. By this reasoning, toroidal fields in the tachocline seem unlikely to exceed 10 kG by very much.

Gilman (2018) showed that for a solar differential rotation DR = 0.28, at all latitudes where the vertical angular velocity gradient in the tachocline is negative, there is a vigorous magnetorotational instability that dominates over magnetic buoyancy instability for peak toroidal fields up to at least 1 kG. He argued that this instability is likely to prevent the solar dynamo from building multi-kilogauss fields in these latitudes, because they will exit the tachocline and rise through the convection zone before they get that large, since the growth rates of magnetorotational instability are so high, particularly

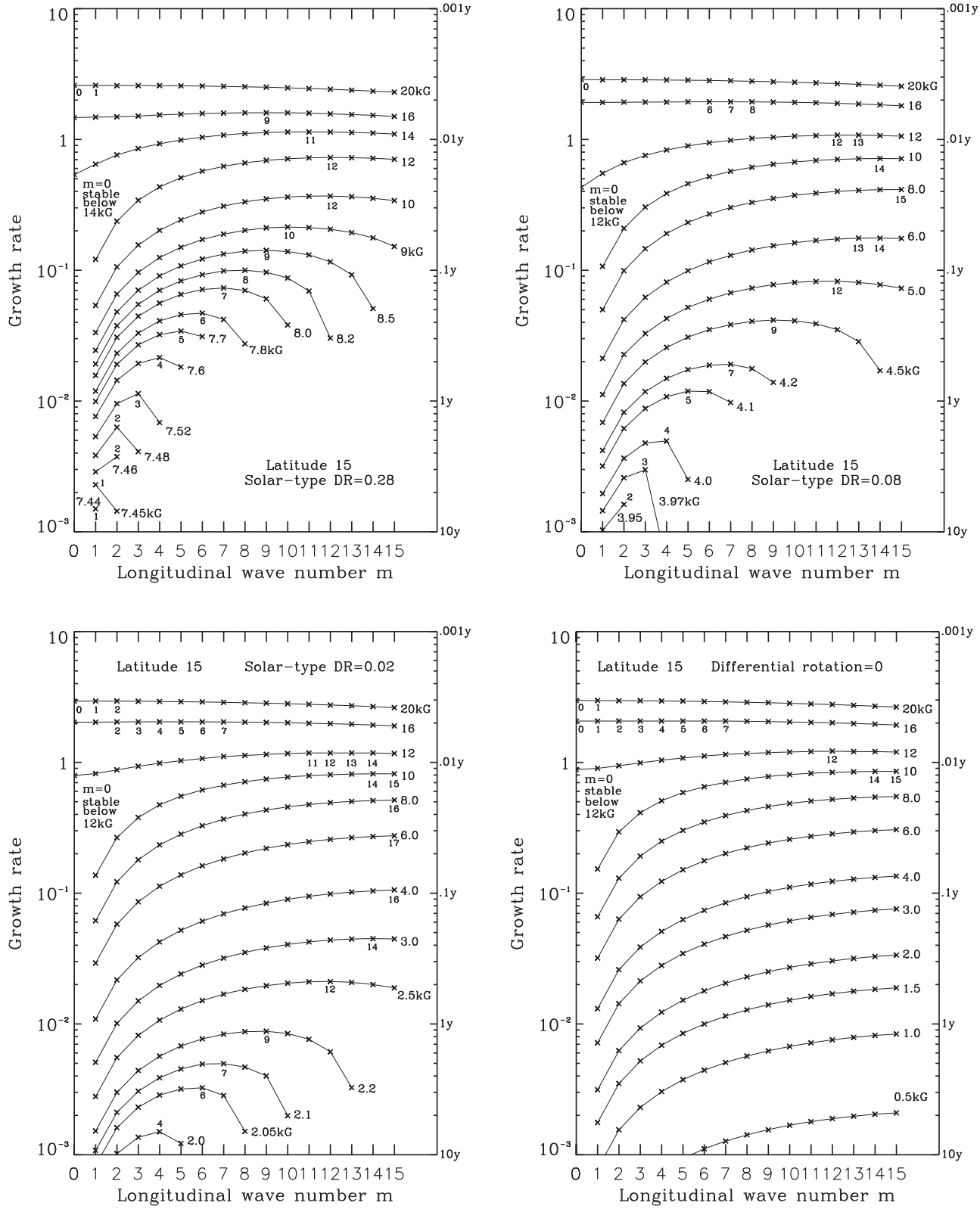

Figure 6. Growth rates of unstable modes at latitude 15° for wavenumbers $m = 0$–15, for selected toroidal fields (labeled at high-m edge of each set of connected points, denoted by crosses) above the instability boundary, for solar-type tachocline differential rotations of 0.28 (top left), 0.08 (top right), 0.02 (bottom left), and 0.0 (bottom right). Most unstable m for each toroidal field chosen is indicated by its integer value. Integers label the most unstable m for each toroidal field. The left-hand scale is dimensionless growth rate; the right-hand scale is dimensional e-folding time in years.

for high longitudinal wavenumber. How general is this result, for other assumed solar-type differential rotations? Figure 7 gives the answer. Here we display growth rates of unstable modes at latitude 55°, typical of high latitudes. In the top left panel, we see that growth rates show very similar structure for all differential rotations shown, from 0.02 to 0.44. In all cases

the growth rate increases linearly with m up to $m > 100$, reaching e-folding growth times (right-hand scale) of less than a tenth of a year, for higher differential rotations much less. These growth rate curves are in two groups, for low and high differential rotations, because at this latitude the lower differential rotation group is stable to hydrodynamic disturbances, which works against the magnetorotational instability, while the higher differential rotations are marginally stable to hydrodynamic rotational instability, so there is no restoring force for the magnetorotational instability to overcome. As explained in Gilman (2018), we reasoned that the purely hydrodynamic instability would be neutralized in the tachocline by thickening it until the gradient is reduced to a value that is at the threshold for hydrodynamic instability. For the lower differential rotations, for a given m the growth rate increases approximately as the square root of the differential rotation. This is consistent with the conclusion drawn from hydrodynamic calculations in Section 5 that the magnetic buoyancy force, which for perturbations is proportional to the reference state toroidal field, must increase as the square root of the vertical rotation gradient to cause instability, thereby breaking out of the storage.

The top right and bottom left and right frames display growth rates for the same sample of solar-type differential rotations as shown in Figure 6 for magnetic buoyancy instability in low latitudes, for a wide range of peak toroidal fields. We see from these frames that for a given differential rotation the growth rates for the same longitudinal wavenumber m increase linearly with peak toroidal field, except for high fields at high wavenumbers, for which magnetic buoyancy and magnetic stress effects begin to influence the result. Competition between magnetic buoyancy and magnetorotational effects, especially for lower differential rotation and toroidal field above 100 G, creates fine structure in the eigenvalue with m, but these structures are not physically significant because toroidal field generated by the stellar dynamo would be disrupted and carried into the convection zone above long before the fields amplified to the point that magnetic buoyancy could compete with magnetorotational instability at latitudes where magnetorotational instability is excited. Therefore, we have not attempted to plot this fine structure in detail; in Figure 7 (and also Figure 10), this structure is undersampled. If we had instead used a toroidal field independent of z, none of this fine structure would be present.

We conclude that magnetorotational instability for solar-type tachocline differential rotations occurs at latitudes where the vertical rotation gradient is negative for essentially all possible differential rotation amplitudes. It follows that all stars with tachoclines and solar-type, if not magnitude, differential rotation will have difficulty building toroidal fields of sufficient amplitude in mid- and high latitudes to create starspots there.

9. Magnetic Buoyancy and Magnetorotational Instabilities for Antisolar-type Differential Rotation

If we reverse the sign of the differential rotation (but keep the rotation of the system the same sign), so that the poles rotate faster than the equator, how do the instabilities we have found change? Figures 8–10 give the answer. These are completely analogous, respectively, to Figures 5–7 for solar-type differential rotation. In Figure 8 we see that the threshold for magnetic buoyancy instability to overcome the adverse vertical rotation gradient is now poleward of 32°.3, where the rotation gradient changes sign, all the way to the poles, with a peak toroidal field that can be stored occurring near latitude 55°. This domain of course exists in both the northern and southern hemispheres, so we can infer that starspots in stars with antisolar differential rotation are likely to occur in mid- and high latitudes, perhaps with a peak near 55°, but not in equatorial latitudes. This conclusion is independent of the strength of the differential rotation, but higher differential rotation allows storage of stronger toroidal fields in these latitudes. It is perhaps remarkable that quantitatively the peak fields storable for solar- and antisolar-type differential rotations are so similar. In the antisolar case, what is happening is that, while magnetic buoyancy has a weaker Coriolis force to push against in higher latitudes, the adverse vertical rotation gradient is larger in high latitudes than low ones for the same total differential rotation. Therefore, the net of the two effects is about the same.

Figure 9 displays the detailed growth rates of unstable disturbances at 55° latitude for $0 \leqslant m \leqslant 15$, as in Figure 6 for solar-type differential rotations of the same amplitude. We see that here too the first mode to become unstable as the toroidal field is increased above the threshold is always $m = 1$. Above the threshold, the most unstable m rises to a maximum and then declines, ultimately to $m = 0$, the sooner for weaker differential rotations. The main difference from that of solar-type differential rotations is that the highest m mode that is most unstable is lower than for solar-type differential rotations. The reason for this is simply that at higher latitudes the same m corresponds to a shorter linear distance in longitude. With shorter linear distance the magnetic stresses that oppose magnetic buoyancy are stronger.

Figure 10 displays growth rates for the magnetorotational instability for antisolar-type differential rotation, which now occurs only in low latitudes where the vertical rotation gradient is negative. Here too the growth rates for a given peak toroidal field increase linearly with longitude wavenumber m and linearly with peak toroidal field for a given differential rotation. But unlike for solar-type differential rotations, there is no gap in growth rates between low and high differential rotations. This is because for all examples shown, at 15° latitude the vertical gradient of rotation is always hydrodynamically stable, so there is always an inertial force working against hydrodynamic instability (see Figure 4) for tachoclines of the same thickness. It is true that for the same differential rotation amplitude the antisolar case gives lower growth rates than does the solar case. This is simply because at 15° latitude there is a larger Coriolis force for the instability to work against than there is at 55°. Nevertheless, for all differential rotations studied magnetorotational instability at low latitudes yields very short e-folding growth times for unstable modes there, again preventing the buildup of strong toroidal fields by dynamo action. Here too we see undersampled fine structure in the growth rate at high m when the toroidal field is high and the differential rotation is low. As discussed in the Figure 7 legend and associated text, this fine structure is not physically significant, because magnetorotational instability will prevent toroidal fields from amplifying enough to compete with it.

There do not seem to be very many examples of significant antisolar differential rotation in main-sequence stars in the literature, but model simulations of rotating convecting spherical shells for relatively slow rotation suggest that they should exist (Gilman 1977; Gastine et al. 2014). It is also true

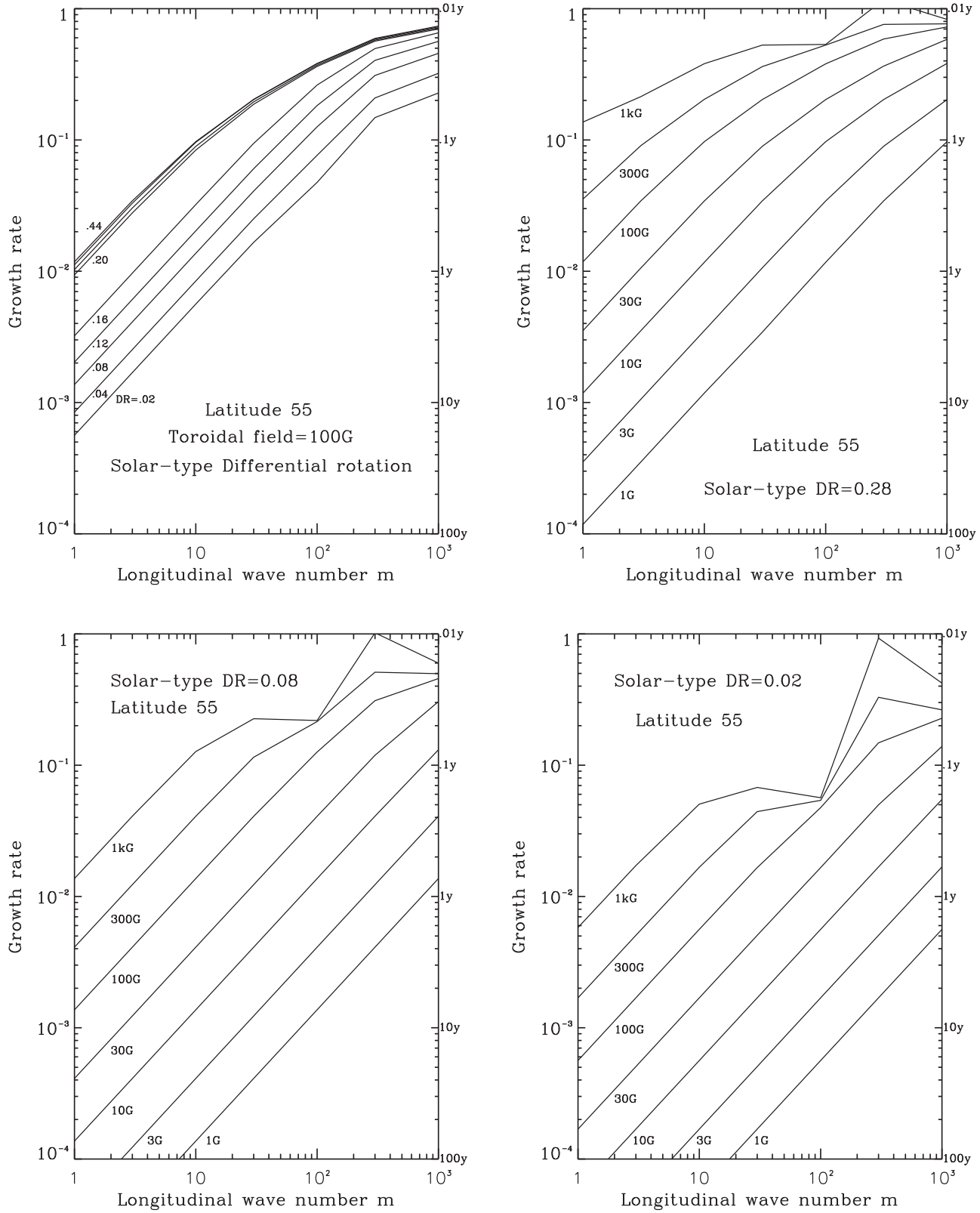

Figure 7. Growth rates of unstable modes at latitude 55° as a function of longitudinal wavenumber m, for a 100 G peak toroidal field, for a range of solar-type differential rotations (top left), for a range of toroidal fields with solar-type differential rotation of 0.28 (top right), for 0.08 (bottom left), and for 0.02 (bottom right). Physically unimportant variations in growth rate for high wavenumber m, high toroidal field, and weak differential rotation are due to undersampling where magnetic buoyancy and magnetorotational effects are competing (see text).

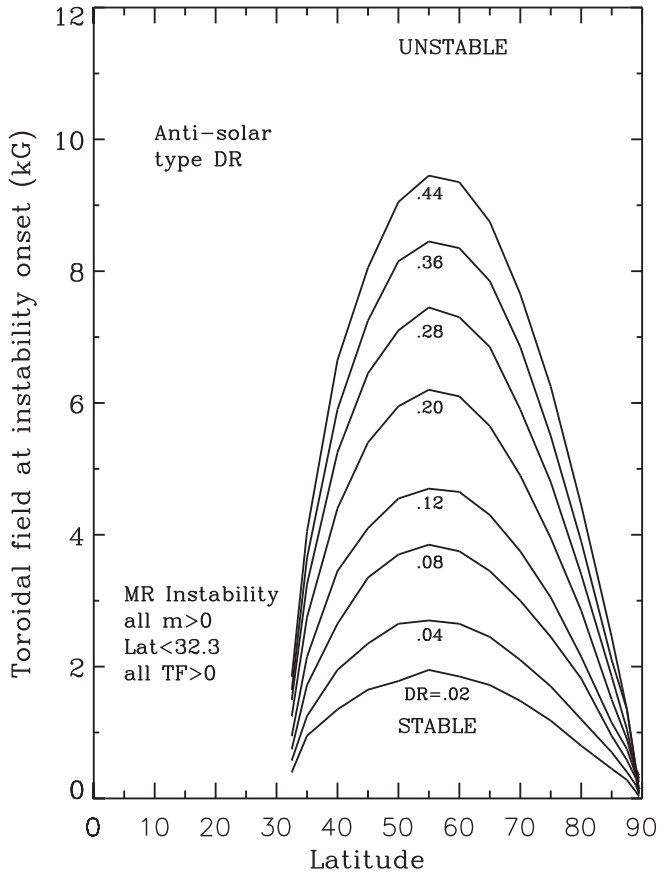

Figure 8. Threshold toroidal field for magnetic buoyancy instability as a function of latitude for a range of antisolar-type tachocline differential rotations.

that stars with deep convection zones rotating relatively fast could show spots in high latitudes, if the trajectories of toroidal flux rising through the convection zone are nearly parallel to the rotation axis. Thus, there may be more than one reason for high-latitude spots in stars.

10. Instability for Weak but Nonzero Differential Rotation

From the top left panels of Figures 7 and 10 one might be tempted to infer that in the limit of differential rotation approaching zero, magnetorotational instability is still present. But this is impossible because there must be differential rotation for this instability to occur. Therefore, for differential rotations less than about 1% of the rotation, there must be a different regime of parameter space to reconcile magnetorotational and magnetic buoyancy instabilities. Figure 11 give results in this domain, again for a peak toroidal field of 100 G, as in Figures 7 and 10. The left panel is for solar-type differential rotation at 55°, the right panel for antisolar-type differential rotation at 15°. For comparison, we have also plotted growth rates for zero differential rotation and for no rotation at all. These two limiting cases both represent strictly magnetic buoyancy instability. From these two limiting cases it is clear that rotation is very inhibiting to magnetic buoyancy instability, since the growth rates with rotation present are two orders of magnitude less than without rotation at all.

We see in Figure 11 that even for differential rotation DR of only 10^{-5} (four orders of magnitude less than the solar differential rotation at tachocline depth!), the vertical rotation gradient has increased the instability growth rates significantly, especially at high longitudinal wavenumber m. By DR $= 10^{-4}$, for m up to about 30, magnetorotational instability has taken over from magnetic buoyancy instability. We know this because, for 10^{-5} and lower, there is instability only in the upper half of the domain, while for 10^{-4}, the entire vertical domain from $z = 0$, 1 is unstable. For still higher m, in the middle of the z domain there is no instability, where differential rotation and magnetic stress effects are opposing each other. In this range of m instability is confined to near both the bottom and top boundaries, resulting in a decline in growth rate with increasing m. As differential rotation is increased still further, to 10^{-3}, the m for which all depths are unstable increases to >100. By 10^{-2} the full depth instability domain boundary is above $m = 200$. Here we see that at high m the magnetorotational instability is so strong that it gives higher growth rates than even for pure magnetic buoyancy instability without either rotation or differential rotation. Obviously this is because we have chosen a relatively modest peak toroidal field of 100 G.

For all cases shown in Figure 11, for $m = 250$ and higher there appears to be a breakdown in accuracy in evaluation of the quartic solutions, even using double precision for the complex number arithmetic. We know this because in the case of no rotation the algebra reduces to a quadratic, for which there are no unstable solutions for this high an m, but the quartic equation in this limit gives instability at all depths, as if there is a differential rotation present when there is not. For lower m the quartic and quadratic equations give identical results. Therefore, we have omitted growth rates on Figure 11 for $m > 200$. For DR $= 2 \times 10^{-2}$ and higher, as shown in Figures 7 and 10, there does not appear to be a significant accuracy problem at high m, presumably because the larger differential rotation leads to coefficients and solutions of the quartic equation set (Equations (5)–(8)) that are not close to values for which the complex arithmetic becomes inaccurate owing to near cancellation of large numbers, or amplification of round-off errors through taking cubes, etc.

From the results shown in Figure 11 we conclude that at latitudes where it occurs at all, for modest toroidal fields, magnetorotational instability overpowers magnetic buoyancy instability even when the vertical differential rotation is far smaller than occurs in the Sun. This only strengthens the conclusion that where magnetorotational instability should occur, it is extremely difficult for a stellar dynamo to build toroidal fields of sufficient amplitude to create starspots at the surface.

11. Differences and Similarities in Instabilities for Solar- and Antisolar-type Differential Rotation

The most obvious and important difference between solar- and antisolar-type differential rotations in our results is that the latitude domains where magnetic buoyancy and magnetorotational instabilities predominate are reversed at about the latitude where the vertical rotation gradient changes sign. Solar-type differential rotation yields magnetic buoyancy instability dominating in low latitudes when the toroidal field is large enough to allow the instability to overcome the adverse vertical rotation gradient, while magnetorotational instability dominates for all weak to moderate toroidal fields in mid- and high latitudes, preventing toroidal fields from getting large enough to be the origin of sunspots or starspots there. For antisolar differential rotations both domains exactly reverse.

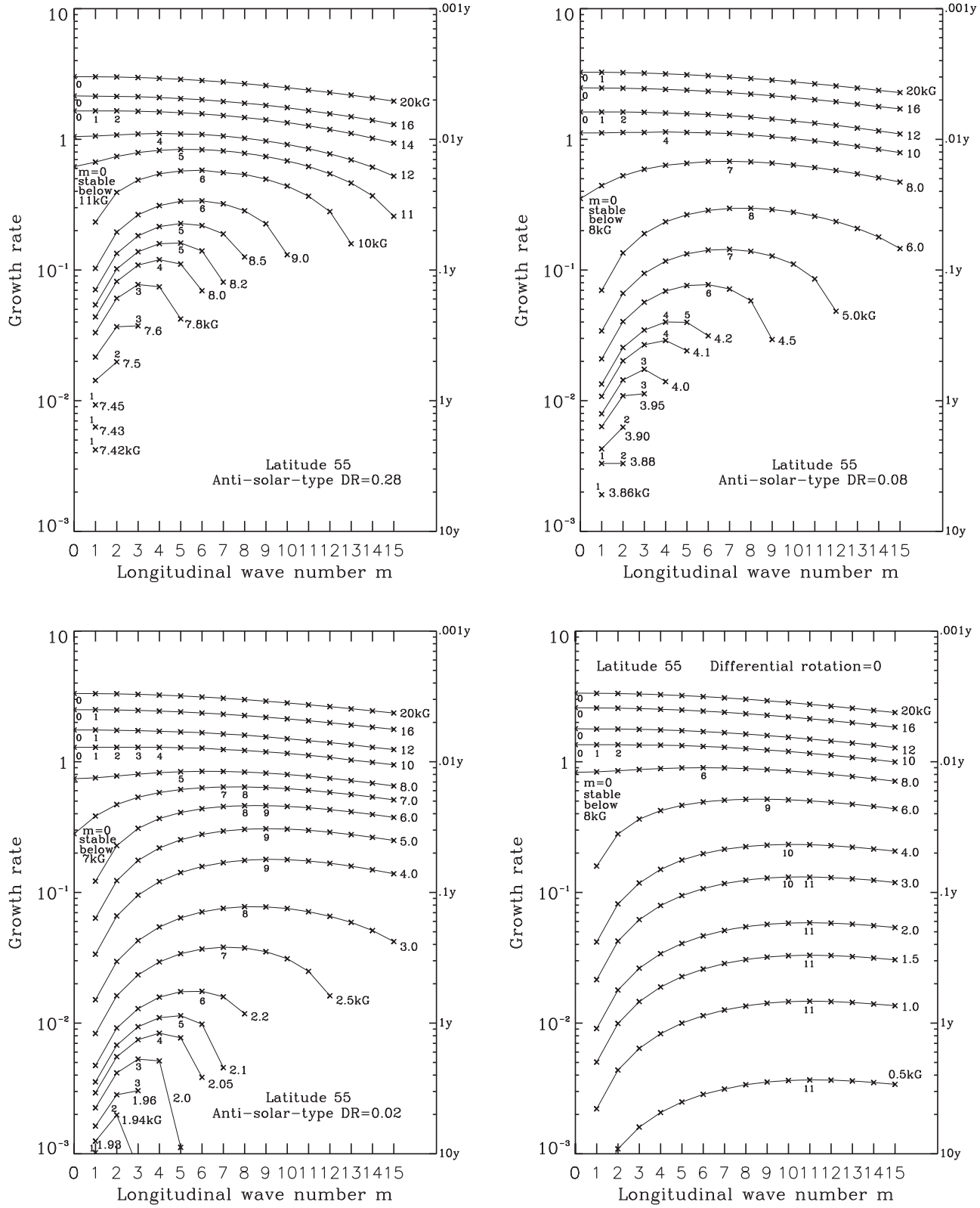

Figure 9. Growth rates of unstable modes at latitude 55° for wavenumbers $m = 0$–15, for selected toroidal fields (labeled at the high-m edge of each set of connected points, denoted by crosses) above the instability boundary, for an antisolar-type tachocline differential rotation of 0.28 (top left), 0.08 (top right), 0.02 (bottom left), and 0.00 (bottom right). Most unstable m for each toroidal field chosen is indicated by its integer value. Integers label the most unstable m for each toroidal field. The left-hand scale is dimensionless growth rate; the right-hand scale is dimensional e-folding time in years.

Despite this major difference, the peak toroidal field that can be stored in the adverse rotation gradient is nearly the same in the two cases. This is illustrated in Figure 12, which presents the peak stored field, at 0° latitude for solar DR and at 55° for antisolar. The difference is less than 20% for all differential rotations. For both solar- and antisolar-type differential rotations, the "square root law" says that the peak toroidal field that can be stored increases as the square root of the

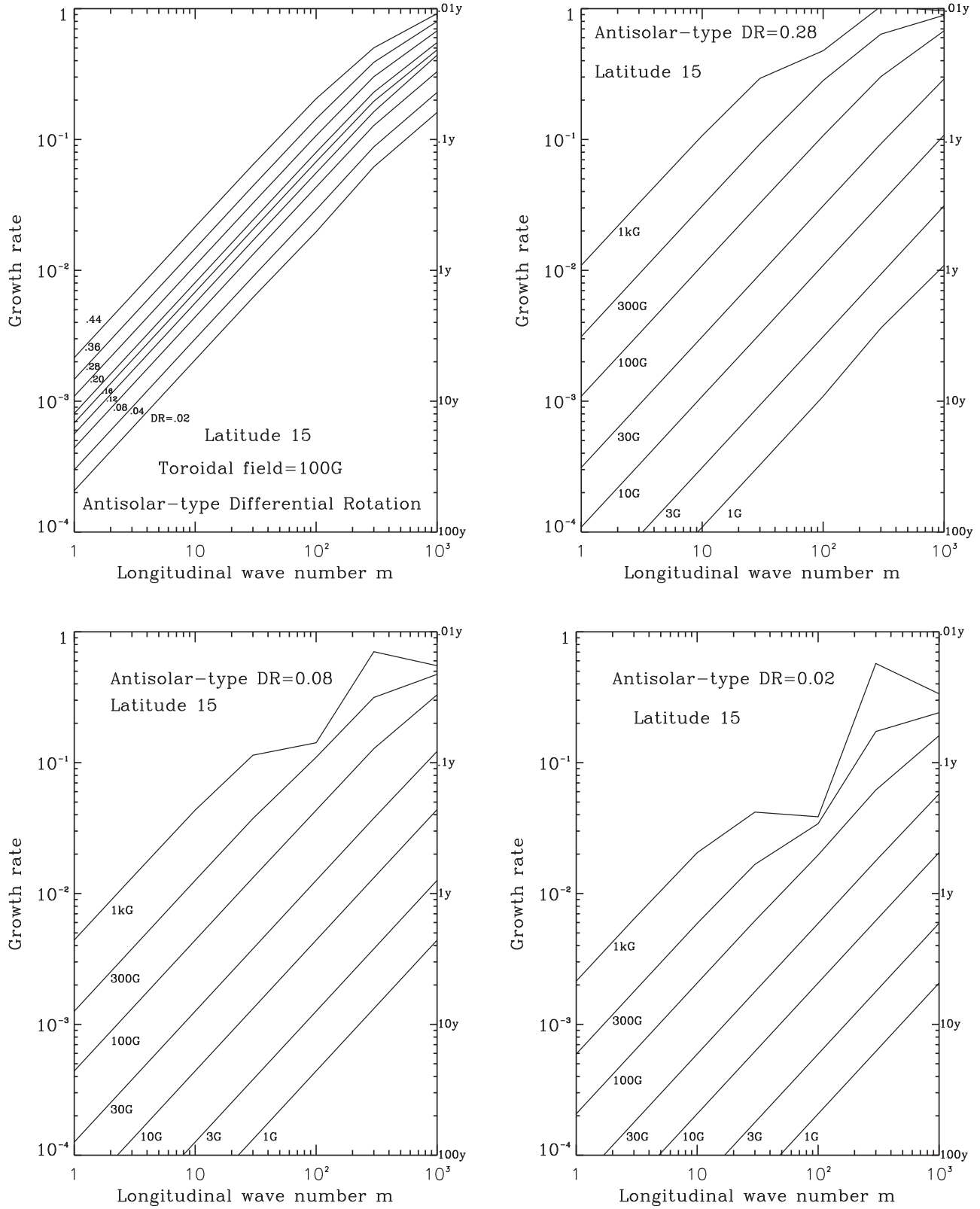

Figure 10. Growth rates of unstable modes at latitude 55° as a function of longitudinal wavenumber m, for a 100 G peak toroidal field, for a range of antisolar-type differential rotations (top left), for a range of toroidal fields with antisolar-type differential rotation of 0.28 (top right), for 0.08 (bottom left), and for 0.02 (bottom right). Departures from straight line growth rate curves at high m and high toroidal field have the same origin as for solar-type differential rotation discussed in the legend for Figure 7 and associated text.

vertical rotation gradient. If we had chosen 15° for the low-latitude toroidal field peak, reasoning that peak fields are very unlikely to be found at the equator for stars with fields predominantly antisymmetric about the equator, as is the Sun's, the difference would be even smaller. Since the toroidal field peak that is possible increases roughly as the square root of the

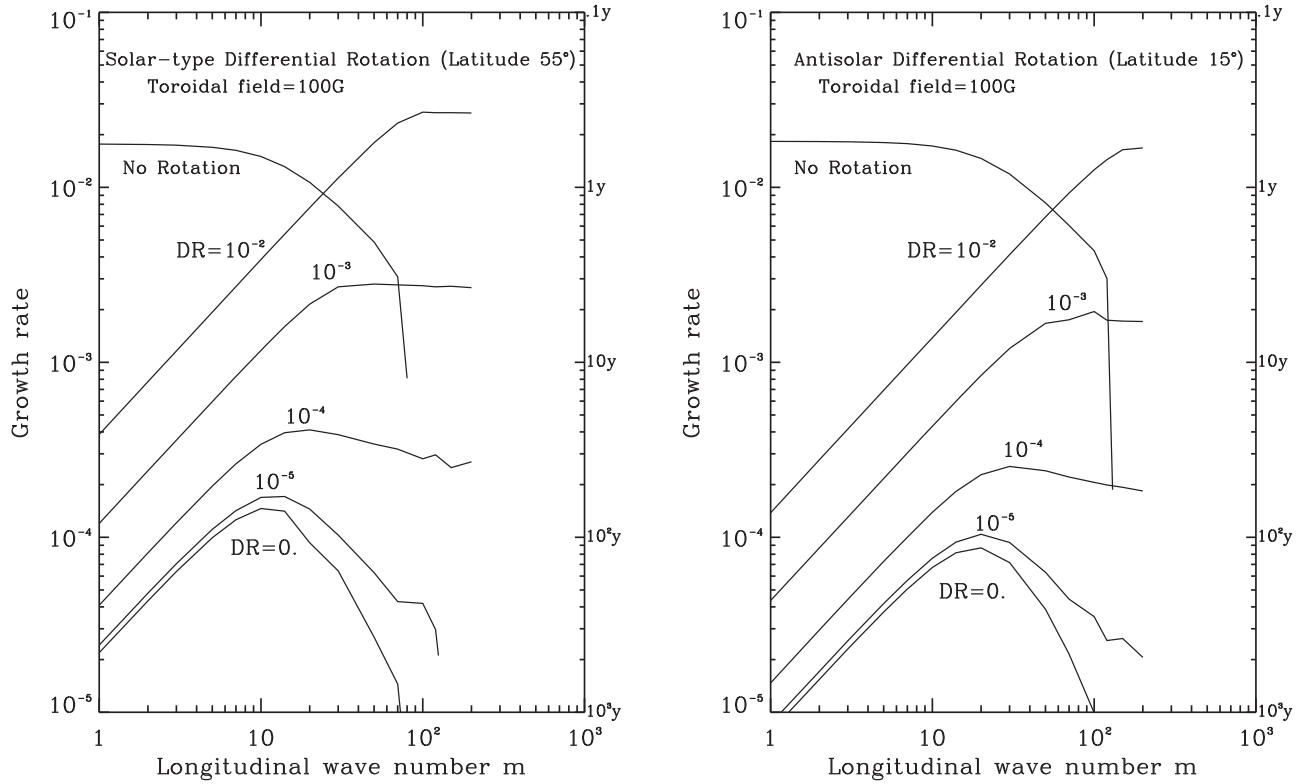

Figure 11. Growth rates of unstable modes with m in the range of 1–200 for very weak solar-type (left panel, at 55° latitude) and antisolar (right panel, at 15° latitude) differential rotation. Growth rates for zero differential rotation and for zero rotation are included for comparison. Note that the vertical scale has been reduced by a factor of 10 compared to analogous results in Figures 7 and 10.

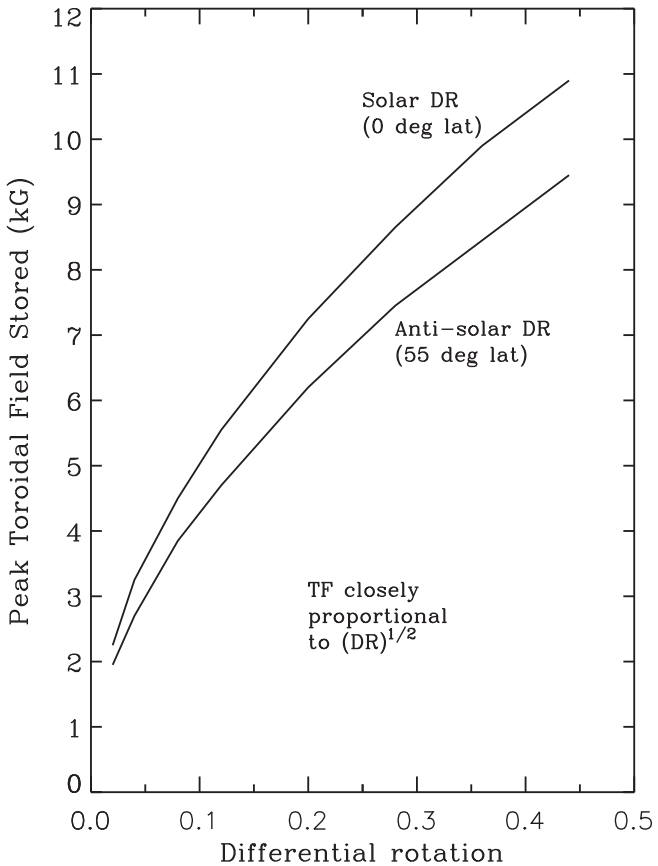

Figure 12. Peak toroidal field stored in tachocline as a function of differential rotation amplitude.

differential rotation, even if the differential rotation were as large as the rotation itself, the peak toroidal field that could be stored via this mechanism could not be more than 20 kG or so for stars with similar rotation and tachocline depth and mass density to the Sun.

The other major similarity between solar and antisolar results is how powerful magnetorotational instability is for even weak differential rotation, easily more powerful than magnetic buoyancy instability for toroidal fields smaller than 1 kG. This power translates into a powerful brake on stellar dynamo action building strong toroidal fields at those latitudes where the vertical rotation gradient is negative.

Other more minor differences between solar and antisolar cases are that growth rates of magnetorotational instability for the same m are lower for antisolar differential rotation because the instability is occurring at lower latitudes where the stabilizing Coriolis force is stronger. Also, hydrodynamic rotational instability requires larger negative vertical rotation gradient in the antisolar than in the solar case for the same reason. Finally, the most unstable magnetically buoyant modes are for smaller m in the antisolar case because they occur at higher latitudes where the physical length in longitude of a given m is shorter.

Taken all together, our results also illustrate how different the roles of rotation and differential rotation are. Rotation is always stabilizing for both magnetic buoyancy and magnetorotational instability, while differential rotation can be either stabilizing or destabilizing, depending on its amplitude, latitude, and sign. As evidenced in Figure 11, the stabilizing effect of rotation can be completely overcome by even a rather modest differential rotation or the right type. This is because pure rotation contains no kinetic energy available to drive an

instability, while differential rotation does, if it can be perturbed in such a way as to release at least some of that energy.

12. Stars with Maximum or Minimum Rotation in Midlatitudes

All results we have shown above are for Sun-like stars with either solar- or antisolar-like differential rotations. But it is very possible that there are intermediate cases for which there is either a minimum or a maximum in angular velocity in midlatitudes (Gilman 1977, 1980). We have not done the calculations, but we can infer qualitatively from our solar and antisolar results some properties of these intermediate cases. The basic "rule" is that toroidal field can only be stored against magnetic buoyancy at those latitudes where the local vertical angular velocity gradient is positive. Therefore, we infer that in stars with maximum angular velocity in midlatitudes, if spots are produced at all, they will also be found in midlatitudes. Conversely, if the minimum angular velocity occurs in midlatitudes, spots will be found, if anywhere, only at low and high latitudes. In reasoning this way, we are assuming, as we did for both solar and antisolar differential rotations, that there is a balance of torques between the stellar convection zone and the radiative, solidly rotating interior below; the signs of the vertical rotation gradients are determined by this balance. No matter what the latitudinal differential rotation is in a stellar tachocline, storage of toroidal field in the stellar tachocline by our rotational mechanism occurs only where the radial gradient is positive.

13. Generalizing Results for Nonsolar Parameters beyond Differential Rotation

Without further calculations we can discuss qualitatively how results would be changed by changing the values of the various scaling parameters summarized in Section 2. For example, how will the peak toroidal fields that can be stored in the tachocline change with various scaling assumptions? Since magnetic fields have been scaled by $R\Omega/\rho_{00}^{1/2}$, the same dimensionless toroidal field can correspond to a quite different dimensional field. For a star with the same tachocline radius, and therefore almost certainly the same tachocline mass density, that rotates twice as fast as the Sun will be capable of storing twice the peak toroidal field for the same percentage differential rotation. This would mean that fields of 16–18 kG could be stored. Conversely, a star with half the solar rotation rate could store only 4–5 kG. Forming starspots should be easier than for the Sun in the high-rotation case but harder in the low-rotation case. For the *Kepler* sample, Reinhold & Gizon (2015) show that a large fraction of active stars have rotation periods substantially smaller than the Sun has, and many of them have differential rotations similar in magnitude (sign undetermined) to the Sun, indicating that such stars should have no trouble storing toroidal fields in their tachoclines until they reach a few tens of kilogauss. On the other hand, at some level of rotation slower than the Sun, theory suggests that no spots will be created, because the toroidal field cannot be stored long enough to build to the amplitude needed to create them. For the fastest-rotating stars in the *Kepler* sample that have the largest relative differential rotation, it is also possible that the peak toroidal field that could be stored could exceed what that star's dynamo could generate, leading to that flux remaining trapped in the tachocline unless some other physical effect comes into play. From our Figures 5 and 8, that could mean that spots would be found nearer the latitude edges of the storage domain, where the peak toroidal field that could be stored would be smaller. It also follows that as the peak toroidal field that can be stored declines, owing, for example, to declining rotation and/or differential rotation, the latitude width of the domain where spots should be found should narrow, concentrated near the equator for solar-type differential rotation, and near 55° latitude for antisolar differential rotations.

For the same stars, the range of radii at tachocline depth is far less, indicating that our results will not change that much for stars of different radii but similar rotation. Since for the Sun the outer 30% of the radius is convective, at tachocline depths the density scale height is a significant fraction of the radius, so for even deeper convection zones, such as in *K* and *M* stars, this density will not increase by more than a factor of three or so. In this case the peak toroidal field storable would increase by only 70% or so. On the other hand, *F* stars are likely to have much shallower tachoclines, where the mass density is small, smaller than in the solar case by one or two orders of magnitude, implying that much smaller toroidal fields could be stored. On the other hand, F stars also tend to be fast rotators, which could compensate in part for the lower mass density. Even so, here again a limit could be reached at which it is not possible to maintain enough toroidal field to create spots.

There are other effects that also limit or increase the storage capability of shallow tachoclines. From Equation (43) of Gilman (2018), the magnetic buoyancy force is roughly proportional to δ^{-2}, unless the shallow tachocline is many scale heights thick, which seems unlikely. This implies that the magnetic buoyancy force will be much larger for the same toroidal field. In turn, this means that magnetic buoyancy from a much smaller toroidal field would still be enough to overcome the effect of a positive vertical rotation gradient there. Therefore, only much smaller toroidal fields could be stored before they emerge as starspots. On the other hand, if the thickness of a shallow tachocline is not much greater than the local scale height, then the much smaller δ than for the Sun implies, from Equation (10), a much larger rotational restoring force for the same rotation difference across the tachocline, implying an increase in peak toroidal field that could be stored. Which effect wins, increased magnetic buoyancy or increased rotational restoring force, depends on the detailed properties of a particular F star. But it is clear that in F star tachoclines, being likely much thinner than that of the Sun, the total amount of toroidal flux, as opposed to peak field, that can be stored must be much less than for the Sun.

The discussion above applies to latitudes where the positive vertical gradient of rotation allows for storage of toroidal flux up to a certain latitude. At all other latitudes, where magnetorotational instability predominates, changing rotation, radius, or tachocline mass density only changes the disturbance growth rates that are achieved. Magnetorotational instability will always control the dynamics, placing strong limits on how strong a toroidal field may become owing to dynamo action. This result appears to be universal for all rotating stars with tachoclines.

So far there are very few *Kepler* sample stars for which details of rotation, differential rotation, and spottedness have been studied. Two examples are reported in Valio et al. (2017)

and Morris et al. (2017). The star Kepler-17 studied in Valio et al. (2017) has a rotation more than twice as fast as the Sun, with a differential rotation percentage of 0.08, compared to 0.28 for the Sun. This suggests that a somewhat larger toroidal field could be stored compared to the Sun, but the radius at tachocline depth is likely to be smaller than for the Sun, reducing that value. Star HAT-P-11 studied in Morris et al. (2017) has almost the same rotation period as the Sun, and a differential rotation probably of similar magnitude and the same sign as the Sun, but a smaller radius and likely much deeper tachocline, being a K star. These effects both favor smaller peak toroidal fields that can be stored.

14. Summary of Instability Results for Stellar Tachoclines

Given the large number of instability and related results we have developed, we summarize here the major findings, and why they are important, in bullet form. These results are conveniently broken into three categories: toroidal field storage, magnetic buoyancy instability, and magnetorotational instability.

Toroidal field storage: important because it provides a mechanism for the stellar dynamo to amplify toroidal fields to the point that when they emerge into the photosphere they are strong enough to form starspots.

1. Occurs only at latitudes where rotation increases outward: low latitudes for solar-type differential rotation, mid- and high latitudes for antisolar-type differential rotation.
2. Peak toroidal field storage is at the equator for solar-type differential rotation, near 55° latitude for antisolar differential rotation.
3. Storage for solar-type differential rotation declines to zero from the equator to the latitude where radial DR changes sign (about 32.°3 latitude in our model).
4. Storage for antisolar-type differential rotation declines to zero at poles and also the latitude where radial rotation gradient changes sign (32.°3).
5. Peak toroidal field that can be stored at a particular latitude is:
   a. proportional to the rotation rate of the interior, for fixed percentage differential rotation at that latitude.
   b. proportional to square root of radial differential rotation for fixed rotation of interior.
   c. proportional to square root of mass density at tachocline depth.

Magnetic buoyancy instability: important because it will inject strong toroidal fields into the stellar convection zone so that they can emerge at the photosphere to form starspots.

1. Occurs for toroidal fields larger than the peak storage value for latitudes that allow field storage, i.e., all latitudes where the rotation rate increases outward.
2. Occurs only where the radial gradient of toroidal field amplitude is negative, i.e., the upper half of the tachocline.
3. Appears for lowest toroidal field near $z = 0.8$, spreading to lower and higher z as toroidal field is increased above critical for instability.
4. Longitude wavenumber $m = 1$ is unstable for lowest supercritical toroidal field.
5. Wavenumber of most unstable mode increases with increasing toroidal field to a peak value, above which it declines to zero for high toroidal fields.
6. Peak growth rate is always near $z = 0.8$, near where the vertical toroidal field gradient is a maximum.
7. Most unstable wavenumber declines from the equator to the poles, for both solar- and antisolar-type differential rotations.
8. e-folding growth time less than a month for even weak radial differential rotation, for toroidal fields less than twice critical for instability.

Magnetorotational instability: important because at latitudes where it occurs it will prevent dynamo-generated toroidal fields from amplifying enough to emerge in the photosphere as starspots; could be the source of less organized photospheric magnetic structures such as ephemeral regions.

1. Occurs only at latitudes where radial rotation gradient is negative, so at mid- and high latitudes for solar-type differential rotation, and low latitudes for antisolar differential rotation.
2. Occurs for all toroidal field amplitudes, even very weak fields.
3. Occurs at all z levels where there is any toroidal field.
4. Growth rates proportional to:
   a. longitude wavenumber m for fixed differential rotation, latitude, and toroidal field.
   b. toroidal field for fixed longitude wavenumber, latitude, and differential rotation, up to the point where magnetic buoyancy effects start to compete with magnetorotational effects.
   c. toroidal field as a function of z for fixed latitude, rotation, and differential rotation.
5. At high longitude wavenumber, e-folding growth time shorter than 0.1 yr for even weak differential rotation and toroidal field no larger than 100 G, much smaller than needed to make a starspot.

15. Implications for Stellar Dynamos

The magnetic buoyancy and magnetorotational instabilities we have described above must connect in some way to the workings of stellar dynamos operating in rotating stars with convection zones and tachoclines. To date, the most successful solar dynamos, which can simulate butterfly diagrams that describe where sunspots should occur as a function of time, are the so-called flux-transport dynamos (Dikpati & Charbonneau 1999; Dikpati et al. 2004, 2010; Dikpati & Gilman 2006; Dikpati 2016). Numerous full 3 MHD simulations of solar and stellar dynamos have also been done, but as yet none of these appear to us to predict well enough the latitude locations of spots, and since most of these models do not even contain true tachoclines, we do not consider them further here. As an aside, we can speculate as to why these simulations have not done very well in reproducing basic solar cycle features such as the butterfly diagram. For one thing, they never seem to simulate correctly the meridional circulation seen at the photosphere, so they are unlikely to get this important dynamical property correctly deeper into the convection zone. This circulation is key to the success of flux-transport dynamos for the Sun; while there is not general agreement from helioseismic observations

on its profile with depth, the latest studies (Mandal et al. 2018) favor a single cell with depth, which works best in solar flux-transport dynamos.

A key ingredient in flux-transport dynamos is the meridional circulation, which advects toroidal and poloidal fields in the meridional plane. On the Sun, this circulation is observed to be poleward at the surface, except at times close to the poles (Ulrich 2010). By mass conservation, there must therefore be return flow at some depth. The flux-transport models that do the best at simulating solar cycle properties are ones in which this return flow is located near the bottom of the convection zone, just above the tachocline. While neither proved theoretically nor measured, it is likely that many if not most stars with significant solar-type differential rotation have qualitatively similar meridional circulations. The effects of magnetic buoyancy and magnetorotational instabilities we have studied should contribute to their dynamos in the following ways.

In mid- and high latitudes, the toroidal field generated and carried toward the equator will be bounded by magnetorotational instability that peels off toroidal flux, which rises to the surface in the form of ephemeral regions. The toroidal field grows only to the point at which the dynamo can sustain the field in the face of this process. As the toroidal field of a given spot cycle moves toward the equator, the intensity of magnetorotational instability declines, as described in detail in Gilman (2018), so the toroidal field peak can rise. Once the toroidal band crosses the latitude where the vertical rotation gradient changes sign, the toroidal field will amplify much more, since the positive rotation gradient prevents it from rising. Once the toroidal field amplifies enough, magnetic buoyancy instability will overcome this constraint, and sunspots should start to appear. It should be possible to include parametrically all these effects into flux-transport dynamo models, by assuming a profile of rising magnetic flux that starts at very low field strength at high latitudes, increasing to much higher fields in low latitudes. Such models already include this kind of process, but generally without a physical basis for a particular profile with latitude.

If somehow the meridional circulation direction were reversed, but with the same differential rotation (a physically unlikely scenario, given simulation results; Gilman 1977, 1980; Gastine et al. 2014), then we would get a star that still had spots in low latitudes, but with a reversed butterfly diagram. But in this case the toroidal field amplification would have to happen very rapidly near the equator to produce low-latitude spots, and then whatever is left when it crosses the zero point in vertical rotation gradient would very quickly come out owing to magnetorotational instability, which might be much more disorganized but perhaps very intense complex field structures. At still higher latitudes, there might be very little flux left to emerge.

For stars with antisolar differential rotation, simulations (Gilman 1977; Gastine et al. 2014) indicate that there could still be meridional circulation of the same sense as in the solar case, perhaps even stronger. This would result in a high-latitude butterfly diagram of similar orientation as for the Sun. Here whatever toroidal flux that did not get to the surface via magnetic buoyancy instability (poleward of 30°–35°) should then come out owing to magnetorotational instability in low latitudes. If in the antisolar case the meridional circulation is also reversed, then there should be a butterfly diagram pattern at high latitudes that is reversed in orientation relative to the solar case.

16. Connections between Instabilities and Stellar Activity

We have produced a theory for magnetic buoyancy and magnetorotational instabilities in stellar tachoclines. But tachoclines are usually way below the visible surface of a star, and many processes not in our model should come into play once the magnetic flux comes into the stellar convection zone. Therefore, a tachocline instability model will not perfectly indicate what magnetic features we should see at the stellar photosphere. In addition, even within the tachocline, we have made certain assumptions that may not always reflect the actual physics of disturbances.

At least three effects within the tachocline should be considered to see how including them might change the results. First, we have assumed isothermal perturbations with very small latitudinal scale. If we take the opposite thermodynamic limit of adiabatic perturbations, the ability of the tachocline to retain toroidal flux goes up. But some way would have to be found to suppress the isothermal modes. One possibility is viscous and ohmic diffusion within the tachocline, but various estimates (Gradski & Mizerski 2018) say that diffusive effects become important only for very small latitudinal scales, for which the perturbations are already isothermal. Another possibility is that the magnetic field being perturbed in the tachocline has a small poloidal component in the reference state, which might create more magnetic stresses to bound the instabilities. This could limit the size of the latitudinal wavenumber, but unless the poloidal component is a significant fraction of the toroidal field, the instabilities we have found could still proceed, but with a slightly different orientation, aligning with the total field.

Once injected into the convection zone, rising flux structures are subject to many processes that can substantially alter their properties before they reach the photosphere, or even destroy the flux pattern altogether. Modeling these effects is way beyond the capabilities of our model. They include at least fragmentation by convective and/or shear turbulence, twisting of tubes, turbulent drag, Coriolis forces, downward drainage of material out of the tube, and coalescence of tube fragments into larger structures near the stellar surface.

A key question to answer is how high amplitude a toroidal field entering the convection zone from the tachocline is needed to retain or rebuild enough coherence and structural integrity to be seen as a starspot at the photosphere. Simulations of rising tubes in the solar convection zone (Weber & Fan 2015 and earlier references cited therein) suggest that this field needs to be at least a factor of 3–4 larger than the peak toroidal field that we have estimated can be stored in the tachocline, held there by the positive vertical rotation gradient. What processes are needed to bridge this gap? Or will more advanced simulations show that such large fields are not necessary? Or can weaker fields be reassembled near the surface to form spots even though the flux rising through the stellar convection zone was largely fragmented? Hale's polarity law for sunspots is virtually always satisfied for the Sun and is virtually certain to apply to other stars with magnetic cycles, so somehow, despite all the disrupting processes at work, the polarity signal gets through to the stellar photosphere from wherever the toroidal fields are amplified and stored.

The role of Coriolis forces in determining the latitudes where starspots should be seen deserves further comment. In general, the faster the star rotates, the more the trajectory of magnetically buoyant, rising magnetic tubes will align with

the stellar rotation axis. Obviously this is much more important for flux entering the convection zone at low latitudes than at high latitudes. Therefore, it is more important for stars with solar-type differential rotation than for antisolar types, because tubes are stored in the solar case at low latitudes. Furthermore, this effect is more important for stars with relatively deep convection zones than for shallow ones, because the rising flux has further to travel parallel to the rotation axis before it reaches the photosphere. In the case of the Sun itself, a flux tube entering the convection zone from the tachocline very near the equator that rose parallel to the rotation axis would appear at the photosphere near latitude 50° or even higher. Clearly this is not what happens, since sunspots are very rarely seen poleward of about 35° at any phase of the cycle. And late in a sunspot cycle, spots are found very close to the equator, so the trajectories of the rising flux tubes that made these spots must have been virtually radial. We conclude that in the case of the Sun, the Coriolis effect is not very large. It could be much larger in stars rotating substantially faster than the Sun but with similar differential rotation. In such a case the band of latitudes where starspots would be seen would be at substantially higher latitudes than predicted from our instability model.

By contrast, stars with antisolar-type differential rotation, for which storage of toroidal field occurs in mid- and high latitudes, would see a smaller change due to the Coriolis effect, because even rising radially the tube trajectories are much closer to parallel with the rotation axis. For example, a tube injected into the convection zone near 55° latitude has a trajectory that is only 35° off from parallel. In any case, Coriolis effects for stars with antisolar differential rotation just reinforce the prediction that surface spots will be seen if at all only in high latitudes.

17. Conclusions and Future Studies

We have shown that in stars with differential rotation and tachoclines, latitudes where the tachocline vertical rotation gradient is positive will store toroidal fields in the tachocline until they be come large enough to break out into the convection zone above via magnetic buoyancy instability. The peak threshold toroidal field for which this breakout occurs is proportional to the square root of this rotation gradient. For the Sun, peak toroidal fields up to about 9 kG can be stored near the equator. Some toroidal field storage by this mechanism occurs even for very weak differential rotation. By contrast, latitudes where the tachocline vertical rotation gradient is positive are subject to vigorous magnetorotational instability even for weak ($\ll$1 kG) toroidal fields, making it very difficult for a stellar dynamo to build toroidal fields of sufficient amplitude to emerge to the stellar photosphere in the form of starspots. But such latitudes could be the location of ephemeral magnetic regions.

These results imply that, in the absence of other processes acting in the tachocline or in the stellar convection zone above, for solar-type latitudinal differential rotations, i.e., ones with fastest rotation at the equator and slowest at the poles, starspots should be seen, if at all, in low latitudes as on the Sun. By contrast, for antisolar-type latitudinal differential rotation, mid- and high latitudes are favored for starspots, perhaps with a peak near 55° latitude. For differential rotation intermediate between these cases, with a maximum or minimum angular velocity in midlatitudes, the same conditions would apply: spots where the tachocline vertical rotation gradient is positive, spots absent at latitudes where this gradient is negative.

In fast-rotating stars (substantially faster than the Sun), Coriolis forces acting on toroidal flux tubes rising through the convection zone may shift the latitude of spot emergence poleward. This effect is most important for solar-type differential rotations, because there the rising flux tube trajectories would be tilted further poleward from a radial path.

Many processes not included in our instability model, or that can occur in the convection zone above the tachocline, could alter these conclusions. Of particular importance is that many 3D MHD simulations of rising flux tubes in the convection zone indicate that peak toroidal fields need to be in the range of a few tens of kilogauss to arrive at the photosphere in coherent form to create spots. Thus, there may be a gap of 20–30 kG between the peak storage of toroidal fields we have found and what is needed to produce spots, at least for stars with similar magnitude differential rotation amplitude to that of the Sun, or smaller. On the other hand, stars that rotate four times faster and have the same percentage differential rotation as the Sun could store toroidal fields four times larger, closing this gap.

For the future, our model should be generalized to include more physical processes in the tachocline, such as viscous and ohmic diffusion, as well as consideration of adiabatic effects and possibly small poloidal fields. But even in their present form, our results can be used to improve parameterizations of toroidal flux leaving the tachocline in solar and stellar dynamo models, and could help provide bottom boundary conditions for 3D MHD simulations of convection in stellar convection zones. It should be useful also to apply our current model to specific stars for which, from observations or stellar interior models, there exists some information about some or all of the following: the star's radius, rotation, differential rotation, depth of its tachocline, and the mass density there, as well as whether it is magnetically active and the latitudes of maximum activity if it is. Our model can be used to reason that a particular star should not be magnetically active, or at least should not have spots. If magnetically active stars are found to have "seasons" within a magnetic cycle (McIntosh et al. 2015; Dikpati et al. 2017, 2018) as the Sun has, then our theory can be used to give guidance on the toroidal field strength to use in stellar tachocline nonlinear oscillation models to simulate these seasons.

The National Center for Atmospheric Research is supported primarily by the National Science Foundation. The author is supported primarily by TIAA. The author thanks Mausumi Dikpati for reviewing the manuscript.

ORCID iDs

Peter A. Gilman https://orcid.org/0000-0002-1639-6252

References

Balbus, S. A. 1995, ApJ, 453, 380
Burington, R. S. 1953, Handbook of Mathematical Tables and Formulas (Sandusky, OH: Handbook Publishers, Inc)
Davies, C. R., & Hughes, D. W. 2011, ApJ, 727, 112
Dikpati, M. 2016, AsJPh, 25, 341
Dikpati, M., Cally, P. S., McIntosh, S. W., & Heifetz, E. 2017, NatSci, 7, 14750
Dikpati, M., & Charbonneau, P. 1999, ApJ, 518, 508
Dikpati, M., deToma, G., Gilman, P. A., Arge, C. N., & White, O. R. 2004, ApJ, 601, 1136

Dikpati, M., & Gilman, P. A. 2006, ApJ, 649, 498
Dikpati, M., Gilman, P. A., deToma, G., & Ulrich, R. 2010, GeoRL, 37, 14107
Dikpati, M., McIntosh, S. W., Bothun, G., et al. 2018, ApJ, 853, 144
Gastine, T., Yadav, R. K., Morin, J., Reiners, A., & Wicht, J. 2014, MNRAS, 438, L76
Gilman, P. A. 1970, ApJ, 162, 1019
Gilman, P. A. 1977, GApFD, 8, 93
Gilman, P. A. 1980, in Proc. IAU Coll. 51, Stellar Turbulence, ed. D. F. Gray & J. L. Linsky (Heidelberg: Springer), 19
Gilman, P. A. 2018, ApJ, 853, 130
Gradski, M. J., & Mizerski, K. A. 2018, ApJ, S235, 13
Kagan, D., & Wheeler, J. C. 2014, ApJ, 787, 21
Mandal, K., Hanasoge, S. M., Rajaguru, S. P., & Antia, H. M. 2018, ApJ, 863, 39
McIntosh, S. W., Leamon, R. J., Krista, L. D., et al. 2015, NatCo, 6, 6491
Menou, K., Balbus, S. A., & Spruit, H. C. 2004, ApJ, 607, 564
Mizerski, K. A., Davies, C. R., & Hughes, D. W. 2013, ApJ, S205, 13
Morris, B. M., Hebb, L., Davenport, J. R. A., Rohn, G., & Hawley, S. L. 2017, ApJ, 846, 99
Parfrey, K. P., & Menou, K. 2007, ApJL, 667, L207
Parker, E. N. 1955, ApJ, 121, 491
Reinhold, T., & Gizon, L. 2015, A&A, 583, A65
Ulrich, R. K. 2010, ApJ, 725, 658
Valio, A., Estrela, R., Netto, Y., Bravo, J. P., & de Medeiros, J. R. 2017, ApJ, 835, 294
Weber, M. A., & Fan, Y. 2015, SoPh, 290, 1295
Yang, S., & Zhang, J. 2014, ApJ, 781, 7